Creep effects on the Campbell response in type-II superconductors

Filippo Gaggioli ⬤, Gianni Blatter ⬤, and Vadim B. Geshkenbein ⬤
Institut für Theoretische Physik, ETH Zürich, CH-8093 Zürich, Switzerland

Applying the strong pinning formalism to the mixed state of a type-II superconductor, we study the effect of thermal fluctuations (or creep) on the penetration of an ac magnetic field as quantified by the so-called Campbell length λ_C. Within strong pinning theory, vortices get pinned by individual defects, with the jumps in the pinning energy (Δe_{pin}) and force (Δf_{pin}) between bistable pinned and free states quantifying the pinning process. We find that the evolution of the Campbell length $\lambda_C(t)$ as a function of time t is the result of two competing effects, the change in the force jumps $\Delta f_{pin}(t)$ and a change in the trapping area $S_{trap}(t)$ of vortices; the latter describes the area around the defect where a nearby vortex gets and remains trapped. Contrary to naive expectation, we find that during the decay of the critical state in a zero-field cooled (ZFC) experiment, the Campbell length $\lambda_C(t)$ is usually nonmonotonic, first decreasing with time t and then increasing for long waiting times. Field cooled (FC) experiments exhibit hysteretic effects in λ_C; relaxation then turns out to be predominantly monotonic, but its magnitude and direction depend on the specific phase of the cooling-heating cycle. Furthermore, when approaching equilibrium, the Campbell length relaxes to a finite value, different from the persistent current, which vanishes at long waiting times t, e.g., above the irreversibility line. Finally, measuring the Campbell length $\lambda_C(t)$ for different states, zero-field cooled, field cooled, and relaxed, as a function of different waiting times t and temperatures T, allows to spectroscopyse the pinning potential of the defects.

I. INTRODUCTION

The phenomenological properties of type-II superconductors subject to a magnetic field B are determined by vortices, linear topological defects that guide the field through the material in terms of quantized fluxes [1] $\Phi_0 = hc/2e$. The interaction of these flux tubes with material defects has a decisive impact on the material's properties, as it determines the amount of current density that the superconductor can transport free of dissipation. This phenomenon, known under the name of vortex pinning [2], has been studied extensively, both in theory and experiment, as one important facet of vortex matter physics [3,4]. Traditional tools to characterize vortex pinning are measurements of critical current densities j_c and full current-voltage (j-V) characteristics [2], as well as the penetration of a small ac magnetic test-field that is quantified through the so-called Campbell penetration length [5] λ_C. In characterizing the pinning properties of the material's mixed state, the Campbell length λ_C assumes a similar role as the skin depth δ (determining the resistivity ρ in the normal state) or the London penetration depth λ_L (determining the superfluid density ρ_s in zero magnetic field). Although well established as an experimental tool, a quantitative calculation on the basis of strong pinning theory [6–8] of the ac Campbell response

has been given only recently [9]. In this paper, we extend this "microscopic" description of the Campbell penetration to include effects of thermal fluctuations, i.e., creep.

The penetration of an ac magnetic field into the mixed state of a superconductor has been first analyzed by Campbell [5], see also Refs. [10,11]. This phenomenological theory relates the Campbell length $\lambda_C \propto B/\sqrt{\alpha}$ to the curvature α of the pinning potential that is probed by small-amplitude oscillations of the vortices. Applying strong pinning theory to this problem provides a lot of insights on the pinning landscape: Within the strong pinning paradigm, vortices exhibit bistable configurations in the presence of a defect. These bistable configurations describe pinned and unpinned (meta)stable states, see Fig. 1, with a finite pinning force density F_{pin} resulting from an asymmetric occupation of the corresponding branches. While the critical current density $j_c \propto \Delta e_{pin}$ is determined by the jumps in energy Δe_{pin} between pinned and unpinned states at (de)pinning [6–8], it turns out [9,12] that the Campbell length $\lambda_C \propto 1/\sqrt{\Delta f_{pin}}$ is given by the jumps in the pinning force Δf_{pin}. Interestingly, the relevant jumps Δf_{pin} determining λ_C depend on the vortex state, e.g., the critical (or zero-field cooled, ZFC) state first defined by Bean [13] or the field cooled (FC) state. Even more, the pinned vortex state depends on the time-trace of its experimental implementation, that leads to hysteretic effects in λ_C as shown in Refs. [9,12] both theoretically and experimentally.

When including thermal fluctuations in the calculation of the pinning force density F_{pin}, different jumps $\Delta e_{pin}(t)$ in the pinning energy become relevant that depend on the time t evolution of the vortex state due to creep. While this relaxation time dependence leads to the decay of the persistent current
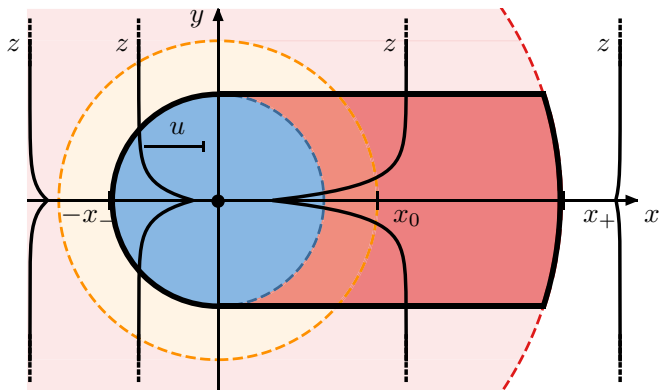
FIG. 1. Vortex- and trapping geometries under strong pinning conditions; note the different meaning of vertical axes referring to the vortices (z) and the trapping area (y), respectively. Shown are vortex configurations $u(z)$ (black solid lines) on approaching the defect head-on (on the x-axis) near the bistable interval $[-x_-, x_+]$. Four stages are highlighted, the (weakly deformed) free state before pinning at $x < -x_-$, pinned on the left at $-x_- < x < 0$, pinned on the right at $0 < x < x_+$, both strongly deformed, and free at $x > x_+$ after depinning. Note the asymmetry in the pinning (at $-x_-$) and depinning (at x_+) processes. In the ZFC state, the trapping area S_{trap} extends over $t_\perp = 2x_-$ along the transverse direction y and over $x_- + x_+$ in the longitudinal one. The total trapping area (with unit branch occupation in the absence of thermal fluctuations) is the sum of the blue and red regions enclosed by the black solid line in the figure. At equilibrium, the branch occupation is radially symmetric with jumps at $R = x_0$, where x_0 denotes the branch crossing point, see Fig. 3; the trapping region (light orange) is enclosed by the orange dashed circumference with radius $R = x_0$. In the FC state, the branch occupation is again radially symmetric and the position of the jump depends on the state preparation. The trapping region is circular, with a radius $x_- \leqslant R \leqslant x_+$; the two extreme cases coincide with the dashed blue circle with $R = x_-$ (phase b in Fig. 5) and the dashed red circle with $R = x_+$ (phase b' in Fig. 5).

density $j(t)$, the corresponding velocity dependence leads to a rounding [14,15] of the transition [16] between pinned and dissipative states in the current-voltage characteristic; again the quantitative nature of the strong pinning description allows for a detailed comparison of the temperature-shifted and rounded excess-current characteristic predicted by theory with experimental data on superconducting films [17].

In the present paper, we determine the Campbell length $\lambda_c(t)$ including the effect of thermal fluctuations. We determine the relevant jumps $\Delta f_{pin}(t)$ in the pinning force which depend on the time t during which the original, e.g., critical, state has relaxed due to creep. For this ZFC situation, we find that the evolution of the Campbell length $\lambda_c(t)$ is the result of two competing effects, the change in the force jumps $\Delta f_{pin}(t)$ and, furthermore, an increase in the trapping area $S_{trap}(t)$ of vortices; the latter describes the area around the defect where a nearby vortex gets and remains trapped, see Fig. 1. Contrary to expectation, we find that for intermediate and very strong pinning, the Campbell length $\lambda_c(t)$ first *decreases* with time t and then starts increasing for long waiting times; at marginally strong pinning, we find $\lambda_c(t)$ decreasing.

Relaxation also appears for the case of field cooled states, as these drop out of equilibrium upon changing temperature and relax when the cooling or heating process is interrupted. In a FC experiment, the Campbell penetration exhibits hysteretic phenomena in a cooling-heating cycle. The relaxation of the Campbell length λ_c then depends on the type of pinning and the location within the hysteresis loop. At intermediate and large pinning, we find three different phases, one where λ_c monotonously decreases with time, one where it monotonously increases towards equilibrium, and a third phase where relaxation is slow due to large creep barriers; at marginally strong pinning, we find λ_c mainly decreasing in time. Several of these findings have been observed in experiments [18,19] and we will discuss them below. We conclude that measuring the Campbell length λ_c for different states, ZFC, FC, and relaxed as a function of different waiting times t, provides insights into the pinning mechanism and gives access to the jumps Δf_{pin} at different locations of the pinning curve, see Fig. 3(c); such measurements and analysis then allow to "spectroscopyse" the pinning potential of defects.

In the following, we first recapitulate relevant aspects of the strong pinning theory and of creep (Secs. II and III that focuses on transport) and then proceed with the calculation of the Campbell penetration depth λ_c in the presence of thermal fluctuations, see Sec. IV. We first focus on the critical (or zero-field cooled, ZFC) state in Secs. IV A and IV B and then extend the analysis to the case of field cooling (FC) in Secs. IV C and IV D. Section V summarizes and concludes our work.

II. STRONG PINNING THEORY

A complete derivation of strong pinning theory starting from an elastic description of the vortex lattice (we assume a lattice directed along z with a lattice constant a_0 determined by the induction $B = \Phi_0/a_0^2$) that is interacting with a random assembly of defects of density n_p has been given in several papers; here, we make use of the discussion and notation in Refs. [8,12,15,20], see also Refs. [21–23] for numerical work on strong pinning. It turns out, that in the low density limit $n_p a_0 \xi^2 \kappa \ll 1$, where ξ denotes the coherence length and κ is the Labusch parameter, see Eq. (4) below, this complex many-body problem can be reduced to an effective single-vortex–single-pin problem. The latter involves an individual flux line with an effective elasticity $\bar{C} \approx \nu\varepsilon(a_0^2/\lambda)\sqrt{c_{66}c_{44}(0)} \sim \varepsilon\varepsilon_0/a_0$ that accounts for the presence of other vortices. Here, $\varepsilon_0 = (\Phi_0/4\pi\lambda_L)^2$ is the vortex line energy, λ_L denotes the London penetration depth, $\varepsilon < 1$ is the anisotropy parameter for a uniaxial material [24], and ν is a numerical, see Refs. [21,23]; the result derives from the elastic Green's function $G_{\alpha\beta}(\mathbf{k})$ of the vortex lattice, see Ref. [24], involving shear (c_{66}) and dispersive tilt ($c_{44}(\mathbf{k})$) and assuming a field that is aligned with the material's axis. Second, the problem involves the pinning potential $e_{def}(\mathbf{r})$ of individual defects; for a point-like defect, $e_{def}(\mathbf{r}) = e_p(\mathbf{R})\delta(z)$ is determined by the form of the vortex core with $e_p(R) = -e_p/(1 + R^2/2\xi^2)$ taking a Lorentzian shape and $\mathbf{R} = (x, y)$ denoting the in-plane coordinate. Below, we will consider a potential of general form whenever possible and focus on Lorentzian-shaped defect potentials $e_p(R)$ in order to arrive
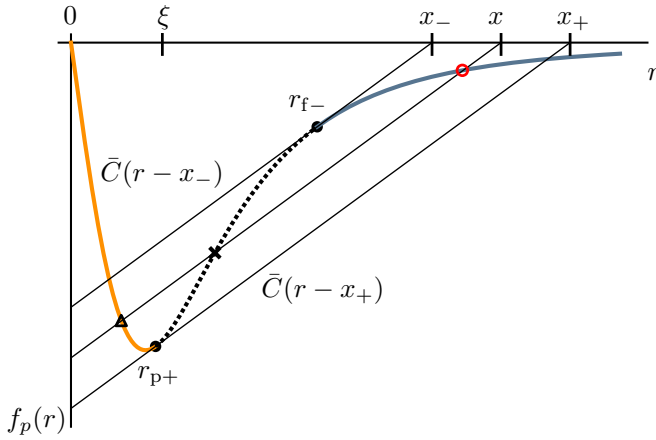
FIG. 2. Graphical illustration [15] of the self-consistent solution of the microscopic force-balance equation Eq. (2) for a Lorentzian potential with $\kappa = 2.5$. When moving the asymptotic vortex position x across the bistable interval $[x_-, x_+]$, we obtain three solutions describing pinned $r_p < \xi$ (orange), free r_f (blue), and unstable r_{us} (black dotted) states. At the edges of the bistable interval, we define the limits $r_p(x_+) \equiv r_{p+}$ and $r_f(x_-) \equiv r_{f-}$ with $f'_p(r_{p+}) = f'_p(r_{f-}) = \bar{C}$ (black solid dots). The tip positions for the pinned ($r_p(x)$, open black triangle) and free ($r_f(x)$, open red circle) branches increase with x, while the unstable one ($r_{us}(x)$, black cross) decreases.

at numerically accurate results; results for non-Lorentzian shaped potentials remain qualitatively the same.

The generic setup involves a vortex line driven along x with asymptotic position $\mathbf{R}_v(z \to \pm\infty) = \mathbf{R}_\infty$ that impacts on the defect located, say, at the origin. The simplest geometry is that of a head-on collision with $\mathbf{R}_\infty = (x, 0)$ and increasing x for an impact from the left; given the rotational symmetry of the defect potential $e_p(R)$, the geometry for the collision at a finite impact parameter y, $\mathbf{R}_\infty = (x, y)$ follows straightforwardly. Assuming a head-on collision to begin with, the geometry simplifies considerably and involves the asymptotic vortex position x and the deformation $u(z)$ of the vortex, see Fig. 1; it turns out, that the problem is fully characterized by its value $u = u(z = 0)$ at the pin, with the vortex line smoothly joining the tip position $r = x + u$ at $z = 0$ with the asymptotic position x at $z \to \pm\infty$, see Fig. 1. The detailed shape $x + u(z)$ of the vortex line then follows from a simple integration [8,12]. The cusp at $z = 0$ is a measure of the pinning strength.

The energy (or Hamiltonian) of this setup involves elastic and pinning energies and is given by

$$e_{\text{pin}}(x, r) = \tfrac{1}{2}\bar{C}(r - x)^2 + e_p(r). \tag{1}$$

Minimizing this energy with respect to r at fixed asymptotic position x, we find the vortex tip position $r(x)$ by solving the nonlinear problem

$$\bar{C}(r - x) = -\partial_r e_p = f_p(r), \tag{2}$$

see Fig. 2 for a graphical solution of this self-consistency problem. This (microscopic) force-balance equation develops multiple solutions when the pin is sufficiently strong, as quantified by the conditions

$$\partial_r^2 e_{\text{pin}} = \bar{C} - f'_p(r) = 0 \quad \text{and} \quad \partial_r e_{\text{pin}} = 0 \tag{3}$$

for the appearance of a local maximum in $e_{\text{pin}}(x, r)$, see Fig. 3(b). The condition (3) defines the Labusch parameter

$$\kappa = \max_r \frac{f'_p(r)}{\bar{C}} = \frac{f'_p(r_m)}{\bar{C}} \tag{4}$$

(with $f''_p(r_m) = 0$ providing the maximal force derivative at r_m) that determines the Labusch criterion

$$\kappa > 1 \tag{5}$$

for strong pinning. Defining the force scale $f_p \equiv e_p/\xi$ and estimating the force derivative or curvature $f'_p = -e''_p \sim f_p/\xi$ produces a Labusch parameter $\kappa \sim e_p/\bar{C}\xi^2$, hence, strong pinning is realized for either large pinning energy e_p or small effective elasticity $\bar{C}$. For the Lorentzian potential, we obtain a maximal force derivative $f'_p(r_m) = e_p/4\xi^2$ at $r_m = \sqrt{2}\,\xi$ and hence $\kappa = e_p/4\bar{C}\xi^2$.

Within the (symmetric) bistable regions $[-x_+, -x_-]$ and $[x_-, x_+]$ opening up at $\kappa > 1$, the force-balance equation Eq. (2) exhibits multiple solutions $r(x)$ corresponding to free (r_f, elasticity dominated) and pinned (r_p, pinning dominated) solutions, see Fig. 2, as well as an unstable solution r_{us} that sets the barrier for creep, see below.

A vortex approaching the defect from the left gets trapped by the pin at $-x_-$ and is dragged towards the pinning center. Upon leaving the defect, the vortex gets strongly deformed, see Fig. 1 and depins at x_+. Inserting the solutions $r_f(x)$, $r_p(x)$, and $r_{us}(x)$ of Eq. (2) back into Eq. (1), we obtain the pinning energy landscape

$$e^i_{\text{pin}}(x) = e_{\text{pin}}[x, r_i(x)] \tag{6}$$

with its multiple branches i = f, p, us shown in Fig. 3(a). The same way, we find the pinning force $f_p[r(x)]$ acting on the vortex tip; inserting the different solutions $r_f(x)$, $r_p(x)$, and $r_{us}(x)$, we obtain the pinning force $f^i_{\text{pin}}(x) \equiv f_p[r_i(x)]$ with its multiple branches i = f, p, us as shown in Fig. 3(c). Note that the pinning force $f_{\text{pin}}(x)$ can be written as the total derivative of the energy $e_{\text{pin}}[x, r(x)]$,

$$f_{\text{pin}}(x) = f_p[r(x)] = -\frac{de_{\text{pin}}[x, r(x)]}{dx}, \tag{7}$$

where we have used the force-balance equation (2) to arrive at the last relation.

The energy $e_{\text{pin}}(x)$ and force $f_{\text{pin}}(x)$ experienced by the vortex are shown in Fig. 3. Due to the presence of multiple branches, we see that a right-moving vortex undergoes jumps in energy Δe_{pin} and force Δf_{pin} at the edges $-x_-$ and x_+ of the bistable intervals (for a left moving vortex, corresponding jumps appear at x_- and $-x_+$). These jumps are the hallmark of strong pinning and determine physical quantities such as the critical current density j_c or the Campbell penetration depth λ_C. In the following, we evaluate the characteristic quantities defining the pinning landscape of Fig. 3 in the limits of very strong ($\kappa \gg 1$) and marginal ($\kappa - 1 \ll 1$) pinning.

1. Bistable interval $[x_-, x_+]$ and extremal tip positions

The extent of the bistable interval $[x_-, x_+]$ is easily found in the very strong pinning limit with $\kappa \gg 1$: With reference to
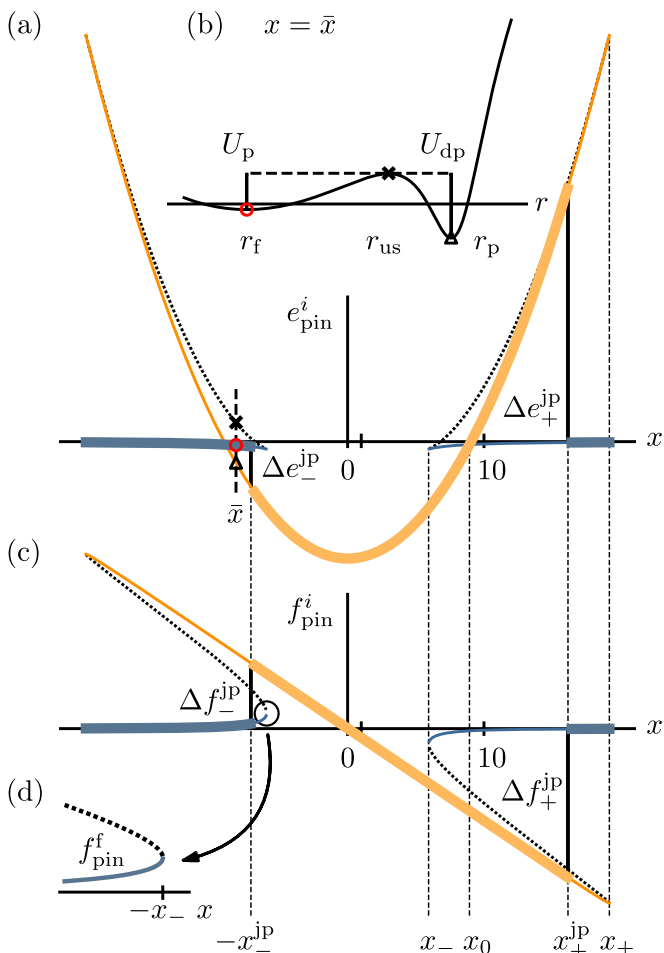
FIG. 3. (a) Multi-valued pinning energy landscape $e_{\mathrm{pin}}^i(x)$, with $i = \mathrm{p, f, us}$ corresponding to the pinned (orange), free (blue), and unstable (dotted) branches for $\kappa = 10$. The vortex coordinate x is expressed in units of ξ. The bistability extends over the intervals $|x| \in [x_-, x_+]$ where the different branches coexist; pinned and unpinned vortex branches cut at the branch crossing point $x = x_0$. (b) Total energy $e_{\mathrm{pin}}(\bar{x}; r)$ versus vortex tip position r for a fixed vortex position $x = \bar{x}$ (dashed vertical line in (a)). The points r_{f} (red dot), r_{p} (black triangle), and r_{us} (black cross) mark the free, pinned, and unstable solutions of the force-balance equation (2). The barriers U_{p} and U_{dp} stabilize the free and pinned states against thermal fluctuations; they coincide in size at the branch crossing point x_0. The maximal pinning force density $F_{\mathrm{pin}} = F_c$ is realized for a maximally asymmetric pinned-branch occupation $p_c(-x_- < x < x_+) = 1$; for the symmetric equilibrium occupation $p_{\mathrm{eq}}(-x_0 < x < x_0) = 1$ the pinning force vanishes. Shown in the figure is the pinned-branch occupation at finite temperatures T (thick colored lines) where thermal fluctuations allow for early pinning at $-x_-^{\mathrm{jp}} < -x_-$ and early depinning at $x_+^{\mathrm{jp}} < x_+$. The corresponding (total) energy jump $\Delta e_{\mathrm{pin}}^{\mathrm{jp}} = \Delta e_+^{\mathrm{jp}} + \Delta e_-^{\mathrm{jp}}$ (vertical black solid lines) determining the pinning force density $F_{\mathrm{pin}}(T)$ is reduced with respect to its critical value (with jumps at $-x_-$ and x_+). (c) Pinning force $f_{\mathrm{pin}}^i(x)$ corresponding to pinned (orange), free (blue), and unstable (dotted) states. The sum of force jumps $\Delta f_{\mathrm{pin}} = \Delta f_-^{\mathrm{jp}} + \Delta f_+^{\mathrm{jp}}$ (vertical black solid lines) determines the Campbell length λ_{C}. (d) The inset shows a zoom of the pinning force $f_{\mathrm{pin}}^{\mathrm{f}}$ near $-x_-$ that contributes to λ_{C} with a steep square-root change in the force jump in the presence of creep, see discussion in Sec. IV B 1.

Fig. 2, we approximate $f_p[r_p(x_+)] \approx f_{p,\max}$ and drop $r_p(x_+) < \xi$ against $x_+ \sim \kappa\xi$ in (2) to find

$$x_+ \approx f_{p,\max}/\bar{C} \sim \kappa\xi. \tag{8}$$

The lower boundary x_- is conveniently obtained from the condition $f_p'[r_{\mathrm{f}}(x_-)] = \bar{C}$. For large κ, we have $r_{\mathrm{f}}(x_-) \gg \xi$ residing in the tail of the pinning potential; assuming a defect potential decaying as $e_p(R) \sim -2e_p(\xi/R)^n$, we obtain

$$r_{\mathrm{f}}(x_-) \approx \xi \left[\frac{2n(n+1)e_p}{\bar{C}\xi^2} \right]^{1/(n+2)} \sim \xi\kappa^{1/(n+2)}. \tag{9}$$

Inserting this result back into Eq. (2), we find that

$$x_- \approx \frac{n+2}{n+1} r_{\mathrm{f}}(x_-). \tag{10}$$

For a Lorentzian potential, we have $f_{p,\max} = (3/2)^{3/2} e_p/4\xi$ and $r_p(x_+) \approx \sqrt{2/3}\,\xi$ and hence

$$x_+ \approx (3/2)^{3/2} \kappa\xi. \tag{11}$$

The lower boundary x_- relates to $r_{\mathrm{f}}(x_-)$ via $x_- \approx (4/3)r_{\mathrm{f}}(x_-)$ and with $r_{\mathrm{f}}(x_-) \approx 2(3\kappa)^{1/4}\xi$, we obtain

$$x_- \approx (8/3)(3\kappa)^{1/4}\xi. \tag{12}$$

The marginally strong pinning case $\kappa \gtrsim 1$ can be quantitatively described via an expansion of the pinning force $f_p(r)$ around the inflection point r_m defined through $f_p''(r_m) = 0$ and using the Labusch parameter in the form $f_p'(r_m) = \kappa\bar{C}$,

$$f_p(r_m + \delta r) \approx f_p(r_m) + \kappa\bar{C}\,\delta r - \gamma\,(e_p/3\xi^4)\delta r^3. \tag{13}$$

We use $\kappa - 1 \ll 1$ as our small parameter and set $\kappa \approx 1$ otherwise [however, beware of additional corrections in $\kappa - 1$ through $\kappa \approx 1 + (\kappa - 1)$]. For a Lorentzian potential, the shape parameter γ assumes the value $\gamma = 3/8$. The cubic expansion (13) is antisymmetric about the inflection point r_m, thus producing symmetric results for pinning and depinning.

The tip locations

$$r_p(x_+) = r_m - \delta r_{\max}, \quad r_{\mathrm{f}}(x_-) = r_m + \delta r_{\max} \tag{14}$$

at (de)pinning are defined by the conditions $f_p[r_{\mathrm{f}}(x_-)] = f_p[r_p(x_+)] = \bar{C}$, see Fig. 2; making use of the expansion (13), we find

$$\delta r_{\max} \approx \frac{\xi}{2}\sqrt{\frac{4\bar{C}\xi^2}{\gamma e_p}}(\kappa - 1)^{1/2}. \tag{15}$$

Inserting this result into the force-balance equation (2) and using (13), we find the boundaries

$$x_\pm = x_m \pm \delta x_{\max} \tag{16}$$

of the bistable region with

$$\delta x_{\max} \approx \frac{\xi}{3}\sqrt{\frac{4\bar{C}\xi^2}{\gamma e_p}}(\kappa - 1)^{3/2}. \tag{17}$$

The pair x_m and r_m of asymptotic and tip positions depends on the details of the potential; while r_m derives solely from the shape $e_p(R)$ and thus does not depend on the elasticity

$\bar{C}$, x_m as given by (2) involves $\bar{C}$ and shifts $\propto (\kappa - 1)$. For a Lorentzian potential, we have

$$r_m = \sqrt{2}\xi, \quad x_m = 2\sqrt{2}\xi + \sqrt{2}\xi(\kappa - 1) \qquad (18)$$

and

$$\delta r_{\max} \approx \xi \, [2(\kappa - 1)/3]^{1/2}, \qquad (19)$$
$$\delta x_{\max} \approx \xi \, [2(\kappa - 1)/3]^{3/2}.$$

Besides the tip positions $r_p(x_+)$ and $r_f(x_-)$ at (de)pinning, we also need the tip positions $r_f(x_+)$ and $r_p(x_-)$ that are not associated with a special point on the free and pinned branches. They are obtained by solving the force-balance equation (2) at $x_\pm = x_m \pm \delta x_{\max}$ using the expansion (13) with the ansatz $r_f(x_+) = r_m + \mu \delta r_{\max}$ and $r_p(x_-) = r_m - \mu \delta r_{\max}$; the resulting equation for μ,

$$\mu + 2/3 - \mu^3/3 = 0, \qquad (20)$$

is solved by $\mu = -1$ ($\rightarrow$ the result (15) obtained before) and $\mu = 2$, hence

$$r_f(x_+) - r_m = r_m - r_p(x_-) \approx 2\delta r_{\max}, \qquad (21)$$

with $\delta r_{\max}$ given in (15).

2. Branch crossing point x_0

At very strong pinning, the bistable region is arranged asymmetrically around the branch crossing point x_0, see Fig. 3; we find the latter by equating the pinning energies (1) for the free and pinned branches: with $x_0 \gg \xi$ at large κ, we have the free and pinned vortex tip positions

$$r_f(x_0) \approx x_0 \quad \text{and} \quad r_p(x_0) \ll \xi, \qquad (22)$$

as follows from the force-balance equation $x_0 - r_f(x_0) = -f_p[r_f(x_0)]/\bar{C}$ (dropping the force term $f_p[r_f(x_0)]$) and Fig. 2. With $e_{\text{pin}}^f(x_0) \approx 0$ and $e_{\text{pin}}^p(x_0) \approx \bar{C}x_0^2/2 - e_p$, we find that

$$x_0 \approx 2\sqrt{2}\xi \left(\frac{e_p}{4\bar{C}\xi^2} \right)^{1/2} \sim \sqrt{\kappa}\xi. \qquad (23)$$

For the Lorentzian potential, we find $x_0 \approx 2\sqrt{2\kappa}\xi$.

When strong pinning is marginal, $\kappa - 1 \ll 1$, the branch crossing point x_0 coincides with x_m. Its location depends on the detailed shape of the potential; for a Lorentzian, we have [see Eq. (18)]

$$x_0 \approx x_m = 2\sqrt{2}\xi + \sqrt{2}\xi(\kappa - 1). \qquad (24)$$

3. Activation barrier U_0

Finally, we briefly discuss the barriers for thermal activation between bistable branches, specifically, the barrier scale U_0 at the branch crossing point. The latter is given by

$$U_0 = e_{\text{pin}}[x_0, r_{\text{us}}(x_0)] - e_{\text{pin}}[x_0, r_f(x_0)]$$
$$= e_{\text{pin}}[x_0, r_{\text{us}}(x_0)] - e_{\text{pin}}[x_0, r_p(x_0)] \qquad (25)$$

and therefore depends on the unstable and pinned/free tip position at x_0. At large $\kappa \gg 1$, the vortex free and pinned vortex tip positions are given in (22). We find the unstable solution r_{us} by using the asymptotic decay $f_p(R) \approx -2n f_p(\xi/R)^{n+1}$

and dropping the term $r_{\text{us}}(x_0)$ against x_0 in the force-balance equation (2), with the result that

$$r_{\text{us}}(x_0) \approx \xi \left(\frac{2n^2 e_p}{\bar{C}\xi^2} \right)^{1/2(n+1)}, \qquad (26)$$

for a Lorentzian potential, $r_{\text{us}}(x_0) \approx 2(\kappa/2)^{1/6}\xi$; indeed, the ratio $r_{\text{us}}(x_0)/x_0 \approx (1/4\kappa)^{1/3} \ll 1$ is parametrically small at large κ. The barrier scale U_0 then evaluates to

$$U_0 \approx \frac{\bar{C}}{2}x_0^2 \approx e_p \qquad (27)$$

with small corrections $\propto 1/\kappa^{n/2(n+1)}$.

In the marginally strong pinning case, we find the tip positions $r = r_m + \delta r$ by solving the force-balance equation (2) with the expansion (13) at $x = x_0 = x_m$, with the three solutions $\delta r = 0$, providing the unstable solution $r_{\text{us}}(x_0) = r_m$, and the free and pinned metastable solutions $r_{f,p}(x_0)$ arranged symmetrically with $\delta r = \pm\sqrt{3}\,\delta r_{\max}$,

$$r_f(x_0) - r_m = r_m - r_p(x_0) = \sqrt{3}\,\delta r_{\max}. \qquad (28)$$

Making use of these results in the definition (25) for U_0 and expanding $e_{\text{pin}}(x_0, r_f = r_m + \sqrt{3}\,\delta r_{\max})$ to fourth order in $\delta r_{\max}$, we find that

$$U_0 \approx \frac{3}{4}\frac{\bar{C}^2\xi^4}{\gamma e_p}(\kappa - 1)^2 = \frac{e_p}{8}(\kappa - 1)^2, \qquad (29)$$

where the last equation applies to the Lorentzian shaped potential. In deriving (29), we have used the expansion (13) as well as the force balance equation (2) to convert the elastic energy $\bar{C}(r_m - x_0)\delta r_{\max}$ to a pinning energy $f_p(r_m)\delta r_{\max}$.

III. TRANSPORT

One of the central features of superconductivity is dissipation-free transport. We briefly discuss the results of strong pinning theory for critical current densities j_c and the effect of thermal fluctuations resulting in a slowly decaying "persistent" current.

The transport properties of a type-II superconducting material is determined by the vortex dynamics as described by the (macroscopic) force-balance equation

$$\eta \mathbf{v} = \mathbf{F}_{\text{L}}(\mathbf{j}) - \mathbf{F}_{\text{pin}}(\mathbf{v}, T), \qquad (30)$$

a nonlinear equation for the mean vortex velocity $\mathbf{v}$, with $\eta = BH_{c2}/\rho_n c^2$ the Bardeen-Stephen viscosity [25] (per unit volume; ρ_n is the normal state resistivity) and $\mathbf{F}_{\text{L}} = \mathbf{j} \times \mathbf{B}/c$ the Lorentz force. The pinning force density $\mathbf{F}_{\text{pin}}$ is directed along $\mathbf{v}$; it depends on the velocity v, that turns finite beyond the critical force density F_c, and on the temperature T driving thermal fluctuations, i.e., creep—we will discuss these effects shortly.

The pinning force density F_{pin} is given by the sum over all force contributions f_{pin}; assuming a uniform distribution of defects, we have to take the average $F_{\text{pin}} = n_p\langle f_{\text{pin}}\rangle$ with the appropriate branch occupation of vortices. For a vortex approaching the defect head-on along x, the free branch terminates at $-x_-$ and the vortex jumps to the pinned branch, gaining the energy $\Delta e_{\text{pin}}^{\text{fp}} = e_{\text{pin}}^f(-x_-) - e_{\text{pin}}^p(-x_-) > 0$ (denoted as Δe_-^{jp} in Fig. 3). Moving forward, the vortex remains

pinned until the branch ends at x_+, where the jump to the free branch involves the energy $\Delta e_{\rm pin}^{\rm pf} = e_{\rm pin}^{\rm p}(x_+) - e_{\rm pin}^{\rm f}(x_+) > 0$ (denoted as $\Delta e_+^{\rm jp}$ in Fig. 3). The critical pinned-branch occupation for head-on trajectories then is $p_c(x) \equiv \Theta(x + x_-) - \Theta(x - x_+)$, while for a finite impact factor y, the branch occupation $p_c(\mathbf{R})$ coincides with characteristic function of the trapping area shown in Fig. 1. The critical branch occupation is maximally asymmetric, what produces the largest possible pinning force. Other branch occupations produce different pinning forces, e.g., the radially symmetric equilibrium occupation $p_{\rm eq}(\mathbf{R}) = \Theta(x_0 - R)$, with x_0 the branch cutting point shown in Fig. 3, leads to a vanishing pinning force.

Averaging the pinning force $\mathbf{f}_{\rm pin}$ over x and y with the vortex population described by the critical branch occupation $p_c(\mathbf{R})$, we obtain the critical pinning force density $\mathbf{F}_c$ [we exploit the anti-symmetry of $\mathbf{f}_{\rm pin}(\mathbf{R})$]

$$\mathbf{F}_c = -n_p \int \frac{d^2\mathbf{R}}{a_0^2} \left[p_c(\mathbf{R})\mathbf{f}_{\rm pin}^{\rm p}(\mathbf{R}) + (1 - p_c(\mathbf{R}))\mathbf{f}_{\rm pin}^{\rm f}(\mathbf{R}) \right]$$
$$= -n_p \int \frac{d^2\mathbf{R}}{a_0^2} p_c(\mathbf{R})[\partial_x \Delta e_{\rm pin}^{\rm fp}(\mathbf{R})]\mathbf{e}_x, \qquad (31)$$

with the energy difference $\Delta e_{\rm pin}^{\rm fp}(\mathbf{R}) = e_{\rm pin}^{\rm f}(\mathbf{R}) - e_{\rm pin}^{\rm p}(\mathbf{R})$ and $\mathbf{e}_x$ the unit vector along x; the y component of the pinning force density vanishes due to the antisymmetry in $f_{{\rm pin},y}$. Following convention, we have included a minus sign in the definition of F_c. The branch-occupation $p_c(\mathbf{R})$ restricts the integral to the trapping area shown in Fig. 1; the integration over x brings forward the constant energy jumps at the two semi-circular boundaries, hence

$$F_c = -n_p \int_{-x_-}^{x_-} \frac{dy}{a_0} \frac{\Delta e_{\rm pin}^{\rm fp}(x,y)}{a_0} \Big|_{x=-\sqrt{x_-^2-y^2}}^{x=+\sqrt{x_-^2-y^2}}$$
$$= n_p \frac{\Delta e_{\rm pin}^{\rm fp} + \Delta e_{\rm pin}^{\rm pf}}{a_0} \int_{-x_-}^{x_-} \frac{dy}{a_0}$$
$$= n_p \frac{t_\perp}{a_0} \frac{\Delta e_{\rm pin}^{\rm fp} + \Delta e_{\rm pin}^{\rm pf}}{a_0}, \qquad (32)$$

where we have defined the transverse trapping length $t_\perp = 2x_-$. The result (32) for the pinning force density shows that all vortices hitting the left-side semi-circle of diameter $t_\perp$ get pinned, see Fig. 1, and contribute equally to the pinning force density, a consequence of the rotationally symmetric pinning potential $e_p(R)$. We confirm that the multi-valued energy landscape in Fig. 3 is central for obtaining a finite pinning force density $F_{\rm pin} \propto n_p$; for $\kappa < 1$ jumps are absent and the integral over the corresponding smooth periodic function $f_{\rm pin}(x)$ in Eq. (32) vanishes. This is the realm of weak pinning with a mechanism that is collective, resulting in a density scaling [8] $F_{\rm pin} \propto n_p^2$.

A. Critical current density j_c

We obtain the critical current density j_c from the force balance (30) by setting $v = 0$ and choosing the maximal pinning force density F_c associated with the most asymmetric branch

occupation $p_c(\mathbf{R})$,

$$j_c = cF_c/B = (c/\Phi_0) n_p t_\perp \Delta e_{\rm pin} \qquad (33)$$

with $\Delta e_{\rm pin} = \Delta e_{\rm pin}^{\rm fp}|_{-x_-} + \Delta e_{\rm pin}^{\rm pf}|_{x_+}$ the sum of (positive) jumps in the pinning energy $e_{\rm pin}(x)$ and $t_\perp = 2x_-$. Note that strong pinning does not necessarily imply a large critical current density j_c, as our approximation of independent pins requires a small density n_p.

B. Creep effects on transport: persistent current

Starting with a nonequilibrium initial state at time $t = 0$, thermal fluctuations (or creep) drive the system towards equilibrium. To fix ideas, we start from a critical or ZFC state (and a head-on collision) characterized by the critical pinned-branch occupation $p_c(x) = \Theta(x + x_-) - \Theta(x - x_+)$ and let it decay through creep; the extension of the result to the 2D situation is straightforward. The presence of thermal fluctuations then increases the probabilities for pinning near $-x_-$ and depinning near x_+, that leads to a reduction of the pinning force density $F_{\rm pin} < F_c$. We account for such thermal hops of vortices into and out of the pin through proper calculation of the thermal pinned-branch occupation probability $p_{\rm th}(x; t, T)$ via solution of the rate equation [15,26,27] (we set the Boltzmann constant to unity, $k_{\rm B} = 1$)

$$\frac{dp_{\rm th}}{dt} = -\omega_{\rm p}\, p_{\rm th}\, e^{-U_{\rm dp}/T} + \omega_{\rm f}\, (1 - p_{\rm th})\, e^{-U_{\rm p}/T}, \qquad (34)$$

where

$$U_{\rm p}(x) = e_{\rm pin}^{\rm us}(x) - e_{\rm pin}^{\rm f}(x), \qquad (35)$$
$$U_{\rm dp}(x) = e_{\rm pin}^{\rm us}(x) - e_{\rm pin}^{\rm p}(x),$$

denote the barriers for pinning and depinning [cf. Eq. (6)] and $\omega_{\rm p}(x)$, $\omega_{\rm f}(x)$ are the corresponding attempt frequencies. It follows from Fig. 3(a) that the barriers $U_{\rm p}(x \to -x_-)$ and $U_{\rm dp}(x \to x_+)$ for pinning and depinning vanish, implying that modifications of the pinned-branch occupation probability are largest near $-x_-$ and x_+ where we can simplify the rate equation (34) by dropping one of the terms. One finds [15], that after a finite waiting time t, thermal fluctuations produce a shift in the jump positions for pinning and depinning [and a small rounding of the steps in $p_{\rm th}(x)$ that we can ignore]: the jump from the free to the pinned branch appears earlier at $-x_-^{\rm jp} < -x_-$ and so does the location of depinning, $x_+^{\rm jp} < x_+$, with the solution of the rate equation (34) well approximated by the step function $p_{\rm th}(x; t, T) \approx \Theta[x + x_-^{\rm jp}(t, T)] - \Theta[x - x_+^{\rm jp}(t, T)]$.

The renormalized jump positions $-x_-^{\rm jp}(t, T)$ and $x_+^{\rm jp}(t, T)$ are determined by the relations [15]

$$U_{\rm p}(-x_-^{\rm jp}) \approx U_{\rm dp}(x_+^{\rm jp}) \approx T \ln(t/t_0), \qquad (36)$$

with the diffusion time $\tau_0 = \pi j_c d^2 / 2c v_{\rm th} B$ (d is the sample dimension) and t_0 to be determined self-consistently [15] from $t_0 = \tau_0 T/(j_c|\partial_j U|)$. Equation (36) tells us, that thermal fluctuations driven by the temperature T can overcome (de)pinning barriers $U_{\rm p(dp)}$ of size $T \ln(t/t_0)$ after a waiting time t. As a result, waiting a time t at temperature T, the pinned-branch occupation probability changes from $p_c(x) \approx 0$ to $p_{\rm th}(x) \approx 1$ at all positions x within the interval $[-x_-^{\rm jp}(t), -x_-]$ and drops

from $p_c(x) \approx 1$ to $p_{th}(x) \approx 0$ for $x \in [x_+^{jp}(t), x_+]$, thereby reducing the asymmetry of the critical occupation probability $p_c(x)$.

The waiting time t then determines the shape of the pinned-branch occupation probability $p_{th}(x; t, T)$: at short times, thermal relaxation is weak and $p_{th}(x; t, T)$ remains close to $p_c(x)$. On the other hand, for finite T and long waiting times $t \lesssim t_{eq} \equiv t_0 \exp(U_0/T)$, with $U_0 = U_p(x_0) = U_{dp}(x_0)$ the barrier at the branch cutting point x_0, see Fig. 3, relaxation is strong and $p_{th}(x; t, T)$ approaches the symmetric equilibrium occupation $p_{eq}(x) = \Theta(x + x_0) - \Theta(x - x_0)$. Going to very long times t beyond t_{eq}, both of the terms in (34) accounting for pinning and depinning hops near x_0 become equally important in establishing the precise equilibrium shape of the pinned-branch occupation probability.

Generalizing from the head-on collision to a finite-impact geometry is straightforward; evaluating the pinning force density Eq. (32) with p_c replaced by p_{th}, we obtain the result

$$F_{pin}(t, T) = n_p \frac{t_\perp^{jp}(t, T)}{a_0} \frac{\Delta e_{pin}^{jp}(t, T)}{a_0}, \tag{37}$$

that depends on the temperature T and the waiting time t. The premature pinning and depinning processes at $-x_-^{jp}$ and x_+^{jp} modify the trapping length $t_\perp^{jp} = 2x_-^{jp} > t_\perp$ and reduce the (sum of) jumps in the pinning energy, $\Delta e_{pin} \to \Delta e_{pin}^{jp} = \Delta e_{pin}^{fp}|_{-x_-^{jp}} + \Delta e_{pin}^{pf}|_{x_+^{jp}}$. For times $t \gg t_0$, the pinning force density (37) takes the analytical form [15]

$$F_{pin}(t, T) = F_c[1 - g(\kappa) \mathcal{T}^{2/3} + \mathcal{O}(\mathcal{T}^{4/3})], \tag{38}$$

with the dimensionless creep parameter $\mathcal{T}$

$$\mathcal{T}(t, T) \equiv \frac{T}{e_p} \ln \frac{t}{t_0}. \tag{39}$$

The exponent 2/3 derives from the vanishing of barriers on approaching the boundaries of the bistable region, $U_{dp,p}(x) \propto |x - x_\pm|^{3/2}$, with the value 3/2 universal for a smooth pinning potential $e_p(R)$; higher-order terms relevant away from the edges $x_\pm$ produce the corrections $\propto \mathcal{T}^{4/3}$ in (38). The coefficient $g(\kappa)$ subsumes all dependencies on the Labusch parameter κ and has been calculated in Ref. [15]; it involves the competing effects of an increasing trapping length $t_\perp^{jp}$ and a decreasing jump in the total pinning energy Δe_{pin}^{jp}. As the latter is the dominating one for not too strong pinning parameters below $\kappa \sim 10^2$, the pinning force density $F_{pin}(t, T)$ usually decreases under the influence of creep. The relative importance of these two effects will be modified in the analysis of the Campbell penetration depth below, where the role of Δe_{pin}^{jp} is replaced by Δf_{pin}^{jp}.

Inserting the result (38) back into the force-balance equation (30), we immediately obtain the persistent current density: in a typical relaxation experiment (i.e., after a short initial waiting time), we can neglect the dissipative term ηv in Eq. (30) and we arrive at the persistent current density in the form

$$j(t, T) \approx cF_c[1 - g(\kappa) \mathcal{T}^{2/3}(t, T)]/B. \tag{40}$$

The result (40) is valid for times $t \ll t_{eq}$. For large times beyond t_{eq}, we go over to the TAFF region (thermally assisted flux flow [28]) where the creep dynamics governed by the slow $\ln(t/t_0)$ behavior turns into a diffusive vortex motion (and thus ohmic response). The vortex front at R_{vf} then moves into the sample following the diffusion law $R_{vf}(t) \sim \text{const.} - \sqrt{D_{TAFF}t}$ with the diffusion constant [24] $D_{TAFF} \sim c^2 \rho_{TAFF}$ and $\rho_{TAFF} \propto \rho_n (B/H_{c2}) \exp(-U_0/T)$. The current decays algebraically, $j \propto 1/\sqrt{t}$ until the sample (of size d) is fully penetrated at $t_{fp} \sim d^2/D_{TAFF}$. Thereafter, the remaining persistent current decays exponentially, $j(t > t_{fp}) \propto \exp(-t/t_{fp})$.

The above scenario applies to the strong pinning paradigm where barriers saturate in the limit of vanishing currents, $j \to 0$. In reality, correlations between different pinning centers are expected to become relevant at very small drives j, implying growing barriers and glassy response instead.

Below, we will study the influence of creep on the linear response under a small external ac magnetic field, that is, again a typical relaxation experiment involving the waiting time t determining the evolution of the vortex state. It will be interesting to see that creep affects the persistent current and the ac penetration depth very differently, with $j(t, T)$ vanishing at long times while $\lambda_C(t, T)$ remains finite.

IV. AC LINEAR RESPONSE

Probing the superconductor with a small ac field $\delta B = h_{ac} \exp(-i\omega t) \ll B_0$ on top of the (large) dc external field B_0 provides us with valuable information on the pinning landscape. Rather than telling about the jumps Δe_{pin} in the energy landscape when measuring j_c, the Campbell penetration depth λ_C informs us about the force landscape, specifically, the jumps Δf_{pin}, see Fig. 3.

Solving the force-balance equation (30) for the displacement field $U(X, t)$ (we denote coarse grained quantities averaging over many vortices with capital letters, see Ref. [29]) assuming a phenomenological ansatz [11] for the pinning force density $F_{pin} = F_0 - \alpha U$, one finds that the ac field penetrates the superconductor over a distance given by $\lambda_C^2(\omega) = B_0^2/[4\pi(\alpha - i\omega\eta)]$. At the low frequencies typical of such penetration experiments, we can drop the dissipative contribution $\propto \eta\omega$ and obtain the phenomenological result

$$\lambda_C(\omega) = \left[\frac{B_0^2}{4\pi \alpha} \right]^{1/2} \tag{41}$$

due to Campbell [11]. In the following, we discuss the Campbell penetration physics within the strong pinning paradigm, first for the zero-field cooled (ZFC) or critical state and subsequently for the field cooled (FC) situation, including also hysteretic effects appearing upon cycling the temperature up and down in the experiment.

A. Campbell penetration depth λ_C in ZFC state

Within our quantitative strong pinning theory, the action of the ac field on the zero-field cooled state is to reshuffle vortices at the boundaries $-x_-$ and x_+, producing a restoring force density proportional to the displacement **U** of the vortices. We compute the change in the pinning force density $\delta \mathbf{F}_{pin}(\mathbf{U})$ by subtracting from (31) the expression with the displaced branch

occupation $p_c(\mathbf{R} - \mathbf{U})$,

$$\delta \mathbf{F}_{\mathrm{pin}}(\mathbf{U}) = -n_p \int \frac{d^2\mathbf{R}}{a_0^2} [p_c(\mathbf{R}) - p_c(\mathbf{R} - \mathbf{U})]$$
$$\times \left[\mathbf{f}_{\mathrm{pin}}^{\mathrm{p}}(\mathbf{R}) - \mathbf{f}_{\mathrm{pin}}^{\mathrm{f}}(\mathbf{R}) \right]$$
$$\approx -n_p \int \frac{d^2\mathbf{R}}{a_0^2} [\nabla p_c(\mathbf{R}) \cdot \mathbf{U}] \Delta \mathbf{f}_{\mathrm{pin}}^{\mathrm{pf}}(\mathbf{R}). \quad (42)$$

With $\mathbf{U}$ directed along x, the scalar product in the last line of (42) is nonvanishing only along the circular sections of the trapping area in Fig. 1; furthermore, the gradient $\nabla p_c(\mathbf{R})$ is strongly peaked (with unit weight) on the circular boundaries and directed parallel to $\mathbf{e}_R$, the radial unit vector. The scalar product then evaluates to

$$-\nabla p_c(\mathbf{R}) \cdot \mathbf{U}$$
$$= [\delta(R - x_-)(\Theta(\phi - \pi/2) - \Theta(\phi - 3\pi/2))$$
$$+ \delta(R - x_+)(\Theta(\phi + \phi_+) - \Theta(\phi - \phi_+))] U \cos\phi \quad (43)$$

with the polar angle ϕ restricted to angles $\pi/2 < \phi < 3\pi/2$ on the left circular segment of the trapping boundary and $-\phi_+ < \phi < \phi_+$ with $\phi_+ = \arcsin(x_-/x_+)$ on the right one. Inserting the expression (43) into (42) and writing $\Delta \mathbf{f}_{\mathrm{pin}}^{\mathrm{pf}}(\mathbf{R}) \equiv -\Delta f(R) \, \mathbf{e}_R$ (with $\Delta f(R)$ the modulus of $\Delta \mathbf{f}_{\mathrm{pin}}^{\mathrm{pf}}(\mathbf{R})$) directed along the radial coordinate, the change in the pinning force density can be evaluated as

$$\delta \mathbf{F}_{\mathrm{pin}} \approx -n_p U \left[\frac{x_- \Delta f(x_-)}{a_0^2} \int_1^{-1} d \, \sin\phi \, [\cos\phi, \sin\phi] \right.$$
$$\left. + \frac{x_+ \Delta f(x_+)}{a_0^2} \int_{-x_-/x_+}^{x_-/x_+} d \, \sin\phi \, [\cos\phi, \sin\phi] \right]$$
$$= -\frac{n_p U}{2a_0^2} [\pi \, x_- \Delta f(x_-) + \theta_+ \, x_+ \Delta f(x_+), 0], \quad (44)$$

with the effective angle $\theta_+ = 2(\phi_+ + \sin\phi_+ \cos\phi_+)$. The expression (44) is originally calculated for a left-shift $U < 0$ of the vortex critical state; after a short initialization period [29], the same result applies for positive displacements as well, and $\delta F_{\mathrm{pin}}(U) = -\alpha_{\mathrm{sp}}(U - U_0)$ with $U_0(X,t) = \max_{t' < t} U(X,t')$, not to be confused with the barrier U_0 at the branch-cutting point x_0.

In the large κ limit, $x_+ \gg x_-$, see Eqs. (11) and (12), and the curvature in the boundary of the trapping region at $R = x_+$ becomes negligible, see Fig. 1. We can then approximate $\phi_+ \approx \sin\phi_+ \approx x_-/x_+ \ll 1$, and the strong pinning expression for the effective curvature α_{sp} in the ZFC state reads

$$\alpha_{\mathrm{sp}} \approx n_p \frac{t_\perp}{a_0} \frac{\frac{\pi}{4} \Delta f_{\mathrm{pin}}^{\mathrm{pf}} + \Delta f_{\mathrm{pin}}^{\mathrm{fp}}}{a_0}, \quad (45)$$

with the force jumps $\Delta f_{\mathrm{pin}}^{\mathrm{pf}} = f_{\mathrm{pin}}^{\mathrm{p}}(-x_-) - f_{\mathrm{pin}}^{\mathrm{f}}(-x_-) > 0$ and $\Delta f_{\mathrm{pin}}^{\mathrm{fp}} = f_{\mathrm{pin}}^{\mathrm{f}}(x_+) - f_{\mathrm{pin}}^{\mathrm{p}}(x_+) > 0$, where we have returned to the original notation for the two jumps at $-x_-$ and x_+ for convenience [i.e., the difference $\Delta f_{\mathrm{pin}}^{\mathrm{fp}}$ is equal to the modulus $\Delta f(x_+)$ in Eq. (44)]. The factor $\pi/4$ in the numerator of (45) has its origin in the different geometries of the circular boundaries at $-x_-$ and at x_+.

In the opposite limit of marginally strong pinning with $\kappa - 1 \ll 1$, $x_- \lesssim x_0 \lesssim x_+$ and the trapping region acquires an approximately circular geometry. The angle ϕ_+ can be expanded as $\phi_+ \approx \pi/2 - \delta\phi_+/2$, with $\delta\phi_+ \ll \pi/2$, allowing to approximate the effective angle θ_+ as

$$\theta_+ \approx \pi + \mathcal{O}(\delta\phi_+^3). \quad (46)$$

The bistable region is symmetric around x_0, see Eq. (16), and we have $\Delta f(x_-) \approx \Delta f(x_+) = \Delta f_{\mathrm{pin}}^{\mathrm{fp}}(x_+)$ as well as $x_0 \approx (x_+ + x_-)/2$, that produces the following simple expression for the Campbell curvature

$$\alpha_{\mathrm{sp}} \approx n_p \frac{\pi x_0}{a_0} \frac{\Delta f_{\mathrm{pin}}^{\mathrm{fp}}(x_+)}{a_0}, \quad (47)$$

where we have again returned to the original notation for the jump at x_+, $\Delta f_{\mathrm{pin}}^{\mathrm{fp}}(x_+) = f_{\mathrm{pin}}^{\mathrm{f}}(x_+) - f_{\mathrm{pin}}^{\mathrm{p}}(x_+) > 0$. The above results differ from those in Ref. [12] in the more accurate handling of the geometry in the trapping boundary, leading to the appearance of θ_+ and factors $\pi/4$.

The derivation (44) applies to the critical state—the corresponding result for other vortex states is obtained by the proper replacement $p_c(\mathbf{R}) \to p(\mathbf{R})$. E.g., for the equilibrium distribution $p_{\mathrm{eq}}(\mathbf{R})$ with a radially symmetric jump at $R \approx x_0$, the result reads

$$\alpha_0 = n_p \frac{\pi x_0}{a_0} \frac{\Delta f_{\mathrm{pin}}^{\mathrm{fp}}(x_0)}{a_0}. \quad (48)$$

Note that, at $\kappa - 1 \ll 1$, the jump $\Delta f_{\mathrm{pin}}^{\mathrm{fp}}(x_0) = f_{\mathrm{pin}}^{\mathrm{f}}(x_0) - f_{\mathrm{pin}}^{\mathrm{p}}(x_0)$ at x_0 is larger (by a factor $2/\sqrt{3}$) than the jumps $\Delta f_{\mathrm{pin}}^{\mathrm{fp}}$ at x_+ or $\Delta f_{\mathrm{pin}}^{\mathrm{pf}}$ at x_-.

Physically, the expressions (45)–(48) describe the *average curvature* in the pinning landscape that, upon integration, is given by the sum of jumps in the pinning force f_{pin}. This should be compared with the *average pinning force* in Eq. (32) that provides the critical force density F_c and is given by the sum of jumps in the pinning energy e_{pin}. Furthermore, the results for the Campbell curvature (45)–(48) involve the precise geometry of the trapping area with its circular boundaries, while the pinning force density (32) depends only on the total width $t_\perp = 2x_-$. The above interpretation of $\alpha_{\mathrm{sp}} \propto \Delta f_{\mathrm{pin}}$ in terms of the *average* curvature naturally relates the strong pinning result to the phenomenological derivation of λ_c by Campbell [11]. Finally, we obtain the microscopic expression for the Campbell penetration depth within strong pinning theory,

$$\lambda_c(\omega) = \left[\frac{B_0^2}{4\pi\alpha_{\mathrm{sp}}} \right]^{1/2}. \quad (49)$$

B. Creep effects on λ_c in ZFC state

At finite temperatures, the analysis of the vortex system's linear response proceeds in a manner analogous to the one above ignoring thermal fluctuations, with the following modifications: (i) the oscillations in the vortex lattice induced by the small *ac* field now reshuffle those vortex lines close to the thermal jump points at $-x_-^{\mathrm{jp}}$ and x_+^{jp}, implying that the relevant jumps in force are $\Delta f_{\mathrm{pin}}^{\mathrm{pf,jp}} = f_{\mathrm{pin}}^{\mathrm{p}}(-x_-^{\mathrm{jp}}) - f_{\mathrm{pin}}^{\mathrm{f}}(-x_-^{\mathrm{jp}}) > 0$
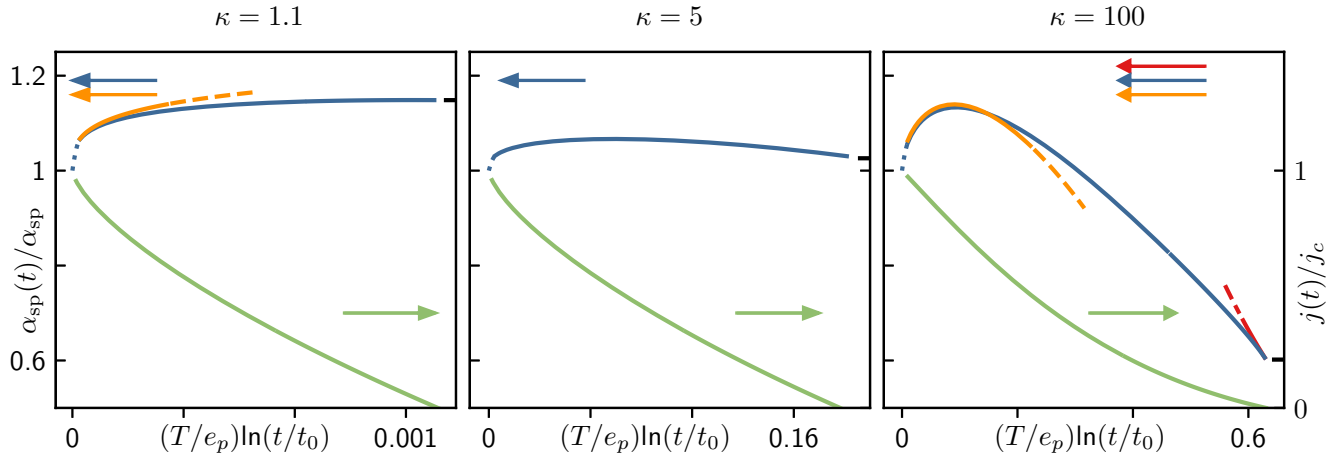
FIG. 4. Comparison of the numeric (blue) and analytic (orange and red) results for the scaled Cambpell curvature (upper part) and the scaled persistent current density $j(t, T)$, Eq. (40) (green, lower part), as a function of the creep parameter in the form of the scaled logarithmic time $(T/e_p) \ln(t/t_0)$. We have assumed a Lorentzian pinning potential with different values of κ. For marginally strong pinning, $\kappa = 1.1$, $\alpha_{sp}(t, T)/\alpha_{sp}$ grows monotonically as a function of time, with a satisfactory agreement between numeric and analytic [Eq. (81)] results; throughout the domain of applicability, the result is dominated by the positive contribution of the curvature in the pinning force branches close to $-x_-$ and x_+. For very strong pinning, $\kappa = 100$, the increase away from zero is dominated by the enhanced trapping length $t_{\perp}^{jp}$; at larger times, the negative contribution to the force jump dominates the behavior, producing a pronounced maximum in the Campbell curvature $\alpha_{sp}(t, T)$ that is visible in both the numeric (blue) and analytic [orange, Eq. (73)] results. The precision in the large κ result is limited in time with deviations showing up when the vortex state approaches equilibrium where the force jumps are close to x_0 rather than $\pm x_\pm$. The red curve is the result Eq. (95) of an expansion around equilibrium that agrees well with the numeric curve. The thick ticks at large times mark the asymptotic value α_0/α_{sp} close to equilibrium $t \sim t_{eq}$ before entering the TAFF region, see text. At intermediate values of the pinning strength, $\kappa = 5$, the increase in $\alpha_{sp}(t, T)/\alpha_{sp}$, originally due to the curvature term in the force jump, gets further enhanced by the increase in trapping length. The (numeric) lines terminate at the boundary of applicability $(T/e_p) \ln(t/t_0) \approx (\kappa - 1)^2/8$ and ~ 1 for marginally and very strong pinning, respectively. At very short times $t \sim t_0$, our creep analysis breaks down as the barriers U vanish. The persistent current density $j(t, T)$ (green) decreases monotonically with time for all three values of κ, approaching the TAFF region at $t \to t_{eq}$ and vanishing in the long-time limit. On the contrary, the curvature $\alpha_{sp}(t, T)$ approaches a finite value α_0 for $t \to t_{eq}$ due to the finite value of the force jump $\Delta f_{pin}^{fp}(x_0)$ at x_0 and then crosses over to the TAFF skin effect.

and $\Delta f_{pin}^{fp, jp} = f_{pin}^f(x_+^{jp}) - f_{pin}^p(x_+^{jp}) > 0$, and (ii) the trapping area involves the renomalized jump locations $x_\pm^{jp}$, producing the thermally renormalized angles $\phi_+^{jp} = \arcsin(x_-^{jp}/x_+^{jp})$ and $\theta_+^{jp} = 2(\phi_+^{jp} + \sin \phi_+^{jp} \cos \phi_+^{jp})$. After a short initialization period, which is not relevant for the present discussion, the field penetration is determined by the effective curvature

$$\alpha_{sp}(t, T) = n_p \left(\frac{\pi}{2} \frac{x_-^{jp}}{a_0} \frac{\Delta f_{pin}^{pf, jp}}{a_0} + \frac{\theta_+^{jp}}{2} \frac{x_+^{jp}}{a_0} \frac{\Delta f_{pin}^{fp, jp}}{a_0} \right). \quad (50)$$

Equation (50) is the central result of this work; it allows us to trace the evolution of the Campbell penetration length $\lambda_C(t, T) \propto 1/\sqrt{\alpha_{sp}}$ as a function of time t during a relaxation experiment. The expression (50) fully characterizes the dependence of α_{sp} on the pinning parameters for times $t \gg t_0$.

At short times and very strong pinning $\kappa \gg 1$, the branch occupation is highly asymmetric and $x_+^{jp} \gg x_-^{jp}$, leading to $\theta_+^{jp} \approx 4\phi_+^{jp} \approx 4x_-^{jp}/x_+^{jp}$. The Campbell curvatures then reads

$$\alpha_{sp}(t, T) \approx n_p \frac{t_\perp^{jp}}{a_0} \frac{\frac{\pi}{4} \Delta f_{pin}^{pf, jp} + \Delta f_{pin}^{fp, jp}}{a_0}, \quad (51)$$

with the thermally enhanced trapping length $t_\perp^{jp} = 2x_-^{jp}$. In the marginally strong pinning limit, we have $\kappa - 1 \ll 1$ and $x_-^{jp} \lesssim x_0 \lesssim x_+^{jp}$, leading to a saturation of the effective angle $\theta_+^{jp} \to \pi$. In this regime, relaxation behaves symmetrically on

both sides of the bistable region with $\Delta f_{pin}^{pf, jp} \approx \Delta f_{pin}^{fp, jp}$, see Eq. (13). Using $x_0 \approx (x_-^{jp} + x_+^{jp})/2$, the Campbell curvature takes a simple form analogous to Eq. (47),

$$\alpha_{sp}(t, T) \approx n_p \frac{\pi x_0}{a_0} \frac{\Delta f_{pin}^{fp, jp}}{a_0}. \quad (52)$$

A numerical evaluation of the Campbell curvature $\alpha_{sp}(t, T)$, Eqs. (50) and (52), as a function of the creep parameter $\mathcal{T} = (T/e_p) \ln(t/t_0)$ at different pinning strengths κ is shown in Fig. 4 (blue lines). For comparison, we also show the decaying persistent current density (40) in the region $j < j_c$. The plots show that $\alpha_{sp}(t, T)$ first increases with time and decreases at long times (but not in the marginal case with κ close to unity). From a phenomenological perspective, this can be understood as a change in the relative occupation of shallow and deep pinning wells in the course of relaxation. Furthermore, we find that, while the persistent current density $j(t, T)$ ultimately vanishes on approaching the equilibrium state, the Campbell curvature $\alpha_{sp}(t, T)$ remains finite and large. We will discuss these findings in detail later; before, we analyze their physical origin with the help of analytic considerations in the limits of moderately strong ($\kappa - 1 \ll 1$) and very strong ($\kappa \gg 1$) pinning.

1. Short and intermediate times

Following Eq. (50), we have to determine the thermally renormalized jumps $\Delta f_{\text{pin}}^{\text{fp,jp}}$ and $\Delta f_{\text{pin}}^{\text{pin,jp}}$ as well as the corresponding trapping parameters. Here, we first analyze the situation at short times $t \ll t_{\text{eq}} = t_0 \exp(U_0/T)$, where the jump positions $-x_-^{\text{jp}}$ and x_+^{jp} remain close to the edges of the bistability intervals $|x| \in [x_-, x_+]$,

$$x_{\pm}^{\text{jp}} = x_{\pm} \mp \delta x_{\pm}, \tag{53}$$

with small asymptotic shifts $\delta x_{\pm} > 0$. Furthermore, we begin our discussion with a study of the very strong pinning regime, where the bistable interval $[x_-, x_+]$ is well separated from the defect potential, as $x_- \sim \kappa^{1/(n+2)}\xi$ and $x_+ \sim \kappa \xi$ are both much larger than ξ, see Eqs. (8)–(10) for more precise expressions for $x_{\pm}$.

In this limit, Eq. (51) for α_{sp} is applicable, with the renormalized trapping length straightforwardly relating to δx_-, $t_{\perp}^{\text{jp}} = 2x_-^{\text{jp}} = t_{\perp} + 2\delta x_-$. Since $\delta x_- > 0$, we find that $t_{\perp}^{\text{jp}} > t_{\perp}$, with thermal fluctuations assisting vortex trapping. Hence, the task of finding $t_{\perp}^{\text{jp}}$ is reduced to the calculation of the shift δx_- in the jump position.

Next, we focus on the total force jump $\Delta f_{\text{pin}}^{\text{jp}} = (\pi/4)\Delta f_{\text{pin}}^{\text{pf,jp}} + \Delta f_{\text{pin}}^{\text{fp,jp}}$. It is convenient to determine the difference in force jumps between the shifted and original jump positions $\pm x_{\pm}^{\text{jp}}$ and $\pm x_{\pm}$ in the form

$$\Delta f_{\text{pin}}^{\text{jp}} - \Delta f_{\text{pin}} \approx \rho[\delta f_{\text{pin}}^{\text{p}}(-x_-^{\text{jp}}) - \delta f_{\text{pin}}^{\text{f}}(-x_-^{\text{jp}})]$$
$$+ \delta f_{\text{pin}}^{\text{f}}(x_+^{\text{jp}}) - \delta f_{\text{pin}}^{\text{p}}(x_+^{\text{jp}}), \tag{54}$$

with $\delta f_{\text{pin}}^{\text{i}}(x_+^{\text{jp}}) = f_{\text{pin}}^{\text{i}}(x_+^{\text{jp}}) - f_{\text{pin}}^{\text{i}}(x_+)$ and $\text{i} = \text{p, f}$, as well as corresponding expressions at $-x_-^{\text{jp}}$. Above, we have introduced the ratio

$$\rho = \pi/4 \tag{55}$$

between the semicircular and rectangular areas appearing in the trapping geometry of Fig. 1, see Eq. (45). Taking a closer look at Fig. 3, we see that the differences in (54) involve a large term $\delta f_{\text{pin}}^{\text{p}}(x_+^{\text{jp}})$ on the linear pinning branch near x_+, a corresponding term $\delta f_{\text{pin}}^{\text{p}}(-x_-^{\text{jp}})$ near $-x_-$, as well as a term $\delta f_{\text{pin}}^{\text{f}}(-x_-^{\text{jp}})$ on the [curved, see Fig. 3(d) inset] free branch near $-x_-$, the remaining term $\delta f_{\text{pin}}^{\text{f}}(x_+^{\text{jp}})$ being obviously small at large κ.

The shifts $\delta f_{\text{pin}}^{\text{p}}$ at $-x_-^{\text{jp}}$ and x_+^{jp} are easily obtained from combining Eqs. (2) and (7),

$$\bar{C}(r - x) = f_p(r) = f_{\text{pin}}(x). \tag{56}$$

With $r_{\text{p}}(x) < \xi$ and $x \in [x_-, x_+] \gg \xi$, we find that $f_{\text{pin}}^{\text{p}}(x) \approx -\bar{C}x$ and

$$\rho \delta f_{\text{pin}}^{\text{p}}(-x_-^{\text{jp}}) - \delta f_{\text{pin}}^{\text{p}}(x_+^{\text{jp}}) \approx \bar{C}(\rho \delta x_- - \delta x_+) \tag{57}$$

follows from the shifts $\delta x_{\pm}$.

For the calculation of the curvature term $\delta f_{\text{pin}}^{\text{f}}(-x_-^{\text{jp}})$, see Fig. 3(d), we have to include both shifts in r and x in (56) and find that

$$\rho \, \delta f_{\text{pin}}^{\text{f}}(-x_-^{\text{jp}}) \approx -\rho \bar{C}(\delta r_{\text{f}-} - \delta x_-), \tag{58}$$

with

$$r_{\text{f}}(x_-^{\text{jp}}) \equiv r_{\text{f}}(x_-) + \delta r_{\text{f}-}. \tag{59}$$

Note that $r_{\text{f}}(x)$ increases with x, see Fig. 2, hence we have $\delta r_{\text{f}-} > 0$ in the above equation. As a result, we obtain the thermal change in force jumps

$$\Delta f_{\text{pin}}^{\text{jp}} - \Delta f_{\text{pin}} \approx \bar{C}(\rho \, \delta r_{\text{f}-} - \delta x_+), \tag{60}$$

leaving us with the task to find the shifts δx_+ and $\delta r_{\text{f}-}$ in the asymptotic and free tip positions, the terms $\pm \rho \bar{C} \delta x_-$ from Eqs. (57) and (58) canceling out.

Next, we determine the shift $\delta r_{\text{f}-}$ in the tip position by expanding the microscopic force balance Eq. (2) around the branch endpoint x_- (where $f_p'[r_{\text{f}}(x_-)] = \bar{C}$) and find that $\delta x_- \approx (|f_p''[r_{\text{f}}(x_-)]|/2\bar{C}) \delta r_{\text{f}-}^2$, hence the tip shift

$$\delta r_{\text{f}-} \approx \left(\frac{2\bar{C}}{|f_p''[r_{\text{f}}(x_-)]|} \delta x_- \right)^{1/2} \tag{61}$$

scales with the square root of the asymptotic shift δx_-. The corresponding result for $\delta r_{\text{p}+} = r_{\text{p}}(x_+) - r_{\text{p}}(x_+^{\text{jp}}) > 0$ involves $f_p''[r_{\text{p}}(x_+)]$.

At large κ, we can evaluate this expression within the tail of the defect potential; assuming, as before, an algebraic decay $e_p(R) \approx 2e_p(\xi/R)^n$, we find that $|f_p''[r_{\text{f}}(x_-)]| \approx \bar{C}(n + 2)/r_{\text{f}}(x_-)$ and relating $r_{\text{f}}(x_-)$ to x_- via Eq. (10), we obtain the shift in the tip position

$$\delta r_{\text{f}-} \approx \frac{\sqrt{2(n+1)}}{n+2} \sqrt{x_- \delta x_-}. \tag{62}$$

Approximating the force jump $\Delta f_{\text{pin}} \approx \bar{C}(x_+ + \rho \, x_-) \approx \bar{C}x_+$ in the absence of fluctuations by its leading term, we arrive at a compact result for the scaled Campbell curvature at large κ,

$$\frac{\alpha_{\text{sp}}(t, T)}{\alpha_{\text{sp}}}$$
$$\approx \left(1 + \frac{\delta x_-}{x_-} \right) \left(1 + \frac{\pi}{4} \frac{\delta r_{\text{f}-}}{x_+} - \frac{\delta x_+}{x_+} \right)$$
$$\approx \left(1 + \frac{\delta x_-}{x_-} \right) \left(1 + \frac{\pi}{4} \frac{\sqrt{2(n+1)}}{n+2} \frac{x_-}{x_+} \sqrt{\frac{\delta x_-}{x_-}} - \frac{\delta x_+}{x_+} \right). \tag{63}$$

Here, the linear terms $\propto \delta x_-/x_-$ and $\propto \delta x_+/x_+$ are universal, while the square-root- or curvature term $\propto \sqrt{\delta x_-/x_-}$ depends on the shape of the defect potential, with the numerical prefactor describing a potential with an algebraic tail decaying as $1/R^n$. The result (63) involves several competing elements: The first factor with a linear correction $\delta x_-/x_-$ is due to the enhanced trapping distance and always leads to an increase in the Campbell curvature $\alpha_{\text{sp}}(t, T)$. On the other hand, the second factor originating from the renormalized force jump contributes with competing terms: while the positive term $\propto \sqrt{\delta x_-/x_-}$ arising from the curvature in $f_{\text{pin}}^{\text{f}}$ at $-x_-$, see Fig. 3(d), is the dominating one at small shifts, i.e., short times, the negative contribution $-\delta x_+/x_+$ deriving from the pinned branch $f_{\text{pin}}^{\text{p}}$ at x_+ becomes relevant at intermediate and larger times.

Note that this competition between trapping area and force jumps appears as well in the discussion of the pinning force density $F_{\mathrm{pin}}(t, T)$ in Eq. (37), but with the force jump Δf_{pin} replaced by the jump Δe_{pin} in pinning energy. This competition has been encoded in the prefactor $g(\kappa)$ of (38) that involves the corresponding two factors related to trapping and energy jumps. However, this time, the total energy jump misses the positive square-root term present in (63) and involves terms linear (negative) and quadratic (positive) in δx_+ [since $e_{\mathrm{pin}} \approx \bar{C}(x_+ - \delta x_+)^2$ for large κ]. It turns out that the negative linear term in the total energy jump dominates over the positive correction in the trapping area, up to very large κ-values beyond $\kappa \sim 10^2$, such that $F_{\mathrm{pin}}(t, T)$ decreases monotonously. Increasing κ beyond this very large value, the situation gets reversed and we find a regime where creep *enhances* the pinning force density, with quite interesting new observable effects that will be discussed in a separate paper [30].

Going beyond small values of δx_-, the result (63) has to be modified, since the square root approximation for $\delta r_{\mathrm{f}-} \propto \sqrt{x_- \delta x_-}$ breaks down. This is easily seen when considering Fig. 3 for larger values of δx_-, where the curvature in the free branch $f_{\mathrm{pin}}^{\mathrm{f}}(x)$ flattens out and $f_{\mathrm{pin}}^{\mathrm{f}}(-x_-^{\mathrm{jp}}) \to 0$ vanishes. In this regime, we have $\delta f_{\mathrm{pin}}^{\mathrm{f}}(-x_-^{\mathrm{jp}}) \approx -f_{\mathrm{pin}}^{\mathrm{f}}(-x_-) = \bar{C}[r_{\mathrm{f}}(x_-) - x_-] \approx -\bar{C}x_-/(n+2)$, where we have used the force balance equation (56) as well as the result (10) for $r_{\mathrm{f}}(x_-)$ and x_-. The result (63) then is replaced by

$$\frac{\alpha_{\mathrm{sp}}(t, T)}{\alpha_{\mathrm{sp}}} \approx \left(1 + \frac{\delta x_-}{x_-}\right)$$
$$\times \left(1 + \frac{\pi}{4}\frac{x_-}{x_+}\left(\frac{1}{n+2} + \frac{\delta x_-}{x_-}\right) - \frac{\delta x_+}{x_+}\right) \quad (64)$$

at large $\delta x_- \gg x_-/2(n+1)$. Note that, while δx_- is parametrically small in κ as compared to δx_+, this is not the case for the ratios $\delta x_-/x_-$ and $\delta x_+/x_+$, since pinning and depinning appear on very different scales x_- and x_+, respectively.

Next, we wish to evaluate the expressions (63) and (64) in terms of experimental parameters, i.e., as a function of temperature T and waiting time t. We first find the shifts $\delta x_\pm^{\mathrm{jp}}$ in the jump positions for the free and pinned branches near $-x_-$ and x_+, respectively. These are determined by the condition (36), telling us that we have to evaluate the depinning and pinning barriers [15] as given by Eq. (35) close to $-x_-$ and x_+, respectively, see Fig. 3(b). The expressions for U_{p} and U_{dp} involve the free and pinned tip position $r_{\mathrm{f}}(x_-^{\mathrm{jp}})$ and $r_{\mathrm{p}}(x_+^{\mathrm{jp}})$ discussed above, cf. Eq. (59), as well as the unstable positions r_{us} at $x_\pm^{\mathrm{jp}}$. The latter are arranged symmetrically with respect to $r_{\mathrm{f}}(x_-)$ and $r_{\mathrm{p}}(x_+)$, $r_{\mathrm{us}}(x_-^{\mathrm{jp}}) = r_{\mathrm{f}}(x_-) - \delta r_{\mathrm{f}-}$ and $r_{\mathrm{us}}(x_+^{\mathrm{jp}}) = r_{\mathrm{p}}(x_+) + \delta r_{\mathrm{p}+}$.

While the shift $\delta r_{\mathrm{f}-}$ is given in Eq. (61), the shift $\delta r_{\mathrm{p}+}$ involves the derivative $f_p''[r_{\mathrm{p}}(x_+)]$ at short distances that depends on the details of the pinning potential. Using the dimensional estimate $f_p''[r_{\mathrm{p}}(x_+)] \sim e_p/\xi^3$, we find that

$$\delta r_{\mathrm{p}+} \sim [(\xi/\kappa)\,\delta x_+]^{1/2}. \quad (65)$$

For a Lorentzian potential, we have the more precise results $f_p''[r_{\mathrm{p}}(x_+)] \approx (3/2)^{7/2}e_p/4\xi^3$ and $\delta r_{\mathrm{p}+} \approx (\sqrt{2}/\kappa)(2/3)^{5/2}\sqrt{x_+ \delta x_+}$. Expanding the pinning/depinning

barriers U_{p} and U_{dp} away from $-x_-$ and x_+, we find the barriers (in compact notation)

$$U \approx \frac{4}{3}\bar{C}\xi^2\sqrt{2\bar{C}/f_p''\xi}\,(\delta x/\xi)^{3/2} \quad (66)$$

where the second derivative f_p'' has to be evaluated at $r_{\mathrm{f}}(-x_-)$ $(r_{\mathrm{p}}(x_+))$ for the pinning barrier U_{p} (the depinning barrier U_{dp}). Focusing on a Lorentzian potential, we arrive at

$$U_{\mathrm{p}}(-x_-^{\mathrm{jp}}) \approx \frac{e_p}{\sqrt{3}\,\kappa^{7/8}}\left(\frac{1}{3}\right)^{3/8}(\delta x_-/\xi)^{3/2}, \quad (67)$$

$$U_{\mathrm{dp}}(x_+^{\mathrm{jp}}) \approx \frac{e_p}{\sqrt{3}\,\kappa^{3/2}}\left(\frac{2}{3}\right)^{9/4}(\delta x_+/\xi)^{3/2}, \quad (68)$$

with contributions from $e_{\mathrm{pin}}'\delta r \propto \bar{C}\,\delta x\,\delta r$ and $e_{\mathrm{pin}}''' \propto \bar{C}\,\delta r^3$. After a waiting time t, thermal fluctuations at temperature T can overcome barriers of size $T\ln(t/t_0)$, rendering smaller barriers ineffective. Making use of Eq. (36) as well as the creep parameter $\mathcal{T}$ defined in (39), we obtain the final results for the thermal shifts

$$\delta x_+ \approx (3/2)^{3/2}\kappa\xi\,(\sqrt{3}\mathcal{T})^{2/3},$$
$$\delta x_- \approx 3^{1/4}\kappa^{7/12}\xi\,(\sqrt{3}\mathcal{T})^{2/3}, \quad (69)$$
$$\delta r_{\mathrm{f}-} \approx 3^{1/4}\kappa^{5/12}\xi\,(\sqrt{3}\mathcal{T})^{1/3}.$$

Indeed, $\delta x_- \sim \kappa^{-5/12}\delta x_+ \ll \delta x_+$ is small, but the ratio $\delta x_-/x_- \approx (3/8)\kappa^{1/3}(\sqrt{3}\mathcal{T})^{2/3}$ dominates $\delta x_+/x_+ \approx (\sqrt{3}\mathcal{T})^{2/3}$ for $\kappa > 19$.

Returning back to the evaluation of the Campbell curvature (63), we find the renormalized trapping length (with the numericals appertaining to a Lorentzian potential)

$$t_\perp^{\mathrm{jp}}(t, T) \approx t_\perp + 2\delta x_-$$
$$\approx t_\perp[1 + (3/8)\kappa^{1/3}(\sqrt{3}\mathcal{T})^{2/3}], \quad (70)$$

where we have used that $t_\perp = 2x_- \approx (16/3)(3\kappa)^{1/4}\xi$ in the last expression. Combining Eqs. (60) and (69), the final result for the renormalized total force jump is

$$\Delta f_{\mathrm{pin}}^{\mathrm{jp}} - \Delta f_{\mathrm{pin}} \approx \kappa\xi\bar{C}[\rho\,3^{1/4}\kappa^{-7/12}(\sqrt{3}\mathcal{T})^{1/3}$$
$$- (3/2)^{3/2}(\sqrt{3}\mathcal{T})^{2/3}]. \quad (71)$$

These results then provide us with an expression for the (scaled) Campbell curvature in the large-κ/small-time limit

$$\frac{\alpha_{\mathrm{sp}}(t, T)}{\alpha_{\mathrm{sp}}} \approx \left(1 + \frac{3}{8}\kappa^{1/3}(\sqrt{3}\mathcal{T})^{2/3}\right)$$
$$\times \left(1 + \frac{\pi}{6}\frac{(4/3)^{1/4}}{\kappa^{7/12}}(\sqrt{3}\mathcal{T})^{1/3} - (\sqrt{3}\mathcal{T})^{2/3}\right), \quad (72)$$

where we have used that $\Delta f_{\mathrm{pin}} \approx \bar{C}(\rho\,x_- + x_+) \approx (3/2)^{3/2}\kappa\xi\bar{C}$, keeping only the leading term in κ. Equation (72) expresses the generic large-κ result (63) in terms of the creep parameter $\mathcal{T}(t, T)$ with the numericals describing the situation for a Lorentzian pinning potential.

Going beyond small values of $\mathcal{T}$, we have to use Eq. (64); the condition $\delta x_- \gg x_-/6$ then translates to a creep parameter $\sqrt{3}\mathcal{T} > (2/3)^3/\kappa^{1/2}$. Evaluating (64) using the thermal shifts

$\delta x_\pm$ in (69), we find the result for larger values of $\mathcal{T}$ to take the slightly modified form,

$$\frac{\alpha_{\rm sp}(t,T)}{\alpha_{\rm sp}} \approx \left(1 + \frac{3}{8}\kappa^{1/3}(\sqrt{3}\mathcal{T})^{2/3}\right)\left[1 + \frac{\pi}{4}\frac{(4/3)^{5/4}}{3\nu\kappa^{3/4}}\right.$$
$$\left. - \left(1 - \frac{\pi}{6}\frac{(4/3)^{1/4}}{\kappa^{5/12}}\right)\frac{(\sqrt{3}\mathcal{T})^{2/3}}{\nu}\right]. \quad (73)$$

In the above result, we have accounted for the improved normalization $\Delta f_{\rm pin} \approx \bar{C}x_+(1 + \rho x_-/x_+) = \bar{C}x_+\nu$ that includes the subdominant term $\rho x_-/x_+$ for better precision, $\nu = 1 + \rho(4/3\kappa^{1/3})^{9/4}$; it is this result that compares well with the numerical result shown in Fig. 4. Finally, the approach to equilibrium with $t \to t_{\rm eq} = t_0 \exp(U_0/T)$ and beyond is discussed in Sec. IV B 2 below.

The above analysis applies to large κ, where the shift in the force jump with its various contributions from free and pinned branches could be physically well motivated. In the following, we focus on the opposite limit of marginally strong pinning $\kappa \gtrsim 1$ with $\kappa - 1$ serving as the small parameter (and setting $\kappa = 1$ otherwise). In this regime, the Campbell curvature $\alpha_{\rm sp}$ is described through Eq. (52), which involves only the force jump $\Delta f_{\rm pin}^{\rm fp, jp}$ at x_+. Making use of the microscopic force balance equation (56), we find the simple formula

$$\Delta f_{\rm pin}^{\rm fp, jp} - \Delta f_{\rm pin}^{\rm fp} \approx \bar{C}[(-\delta r_{\rm f+} + \delta x_+) - (-\delta r_{\rm p+} + \delta x_+)]$$
$$\approx \bar{C}[-\delta r_{\rm f+} + \delta r_{\rm p+}], \quad (74)$$

expressing the change in the total force jump by the shifts in tip positions δr alone. The expressions (61) for the shift in the vortex tip positions $\delta r_{\rm p+}$ and $\delta r_{\rm f-}$ involve the second derivative $f_p'' \approx (e_p/\xi^3)\sqrt{\gamma(\kappa - 1)}$ at the edges $x_\pm$ [obtained with the help of the expansion Eq. (13)] and we find

$$\delta r_{\rm p+} = \delta r_{\rm f-} \approx \left[\frac{4\bar{C}\xi^2}{e_p}\frac{\xi\,\delta x_\pm}{\sqrt{4\gamma(\kappa - 1)}}\right]^{1/2}, \quad (75)$$

symmetric at $r_{\rm p}(x_+)$ and $r_{\rm f}(x_-)$.

Besides the shift $\delta r_{\rm p+}$ associated with the edge of the bistability region, we also need the free tip position near x_+,

$$r_{\rm f}(x_+^{\rm jp}) \equiv r_{\rm f}(x_+) - \delta r_{\rm f+}, \quad (76)$$

that is not associated with a special point on the free branch. It is obtained by evaluating the force-balance equation (2) on the free branch close to x_+,

$$\bar{C}[(r_{\rm f}(x_+) - \delta r_{\rm f+}) - (x_+ - \delta x_+)] = f_p[r_{\rm f}(x_+) - \delta r_{\rm f+}], \quad (77)$$

with the tip position $r_{\rm f}(x_+)$ given in (21). Solving Eq. (77) with the help of the expansion (13), we find the (symmetric) tip shifts expressed through δx_+,

$$\delta r_{\rm f+} [= \delta r_{\rm p-}] \approx [3(\kappa - 1)]^{-1}\,\delta x_+, \quad (78)$$

independent of γ.

Finally, we derive the asymptotic shifts $\delta x_\pm$ using the expansion for the pinning/depinning barriers (66) and find $\delta x_\pm/\xi \approx (e_p/4\bar{C}\xi^2)[4\gamma(\kappa - 1)]^{1/6}(3\mathcal{T})^{2/3}$. This result simplifies considerably when focusing on the Lorentzian potential, where $\delta x_\pm/\xi \approx [3(\kappa - 1)/2]^{1/6}(3\mathcal{T})^{2/3}$.

The renormalized total force jump is obtained by inserting the above tip shifts into Eqs. (74) and we obtain the shift in

the force jumps

$$\Delta f_{\rm pin}^{\rm fp, jp} - \Delta f_{\rm pin}^{\rm fp} \approx \bar{C}\xi\left[\frac{(2/3)^{1/6}(3\mathcal{T})^{1/3}}{(\kappa - 1)^{1/6}} - \frac{(3/2)^{1/6}(3\mathcal{T})^{2/3}}{3(\kappa - 1)^{5/6}}\right], \quad (79)$$

where we have focused on the Lorentzian potential, the generalization to an arbitrary potential being straightforward once the shape parameter γ is known.

To find the total force jump $\Delta f_{\rm pin}^{\rm fp} = \bar{C}[r_{\rm f}(x_+) - r_{\rm p}(x_+)]$ in the absence of fluctuations, we need the free and pinned vortex tip positions at the edge x_+, see Eqs. (15) and (21), that lead us to the result

$$\Delta f_{\rm pin}^{\rm fp} \approx 3\bar{C}\xi\left(\frac{4\bar{C}\xi^2}{e_p}\right)^{1/2}\left(\frac{\kappa - 1}{4\gamma}\right)^{1/2}. \quad (80)$$

The trapping scale x_0 in Eq. (52) depends on the details of the potential, see Sec. II. For the Lorentzian potential, we find the results $\Delta f_{\rm pin}^{\rm fp} \approx 3\bar{C}\xi[2(\kappa - 1)/3]^{1/2}$ and $x_0 \approx \sqrt{2}\xi[2 + (\kappa - 1)]$, see Eq. (18), that takes us to the final result for the curvature at moderately strong pinning $\kappa \gtrsim 1$, to leading order in $\kappa - 1$,

$$\frac{\alpha_{\rm sp}(t,T)}{\alpha_{\rm sp}} \approx 1 + \frac{[(3/2)\mathcal{T}]^{1/3}}{[3(\kappa - 1)]^{2/3}} - \frac{[(3/2)\mathcal{T}]^{2/3}}{[3(\kappa - 1)]^{4/3}}. \quad (81)$$

Note that the last (negative) term is just the square of the second (positive) contribution.

Let us discuss the results (72), (73), and (81) and compare them with the numerical findings, with all of these shown in Fig. 4. First, we translate the time range $1 < t/t_0 \sim \exp(U_0/T)$ where our analysis is valid to the creep variable $\mathcal{T} = (T/e_p)\ln(t/t_0)$, that results in the region $0 < \mathcal{T} < U_0/e_p$. Note that going beyond $t > t_{\rm eq} = t_0\exp(U_0/T)$, we have to include both terms in Eq. (34); instead, here, we simply terminate our approximate analysis with the same result (up to irrelevant details in the form of the steps at $\pm x_0$) for the equilibrium distribution $p_{\rm eq}$.

The barriers U_0 at the branch crossing point x_0 have been derived both for strong and marginal pinning in Sec. II, see Eqs. (27) and (29). We then find our analysis to be valid for values of the creep variable $\mathcal{T}$ inside the ranges

$$0 < \mathcal{T} < 1 \qquad \text{for } \kappa \gg 1, \quad (82)$$
$$0 < \mathcal{T} < (\kappa - 1)^2/8 \quad \text{for } \kappa - 1 \ll 1,$$

resulting in very different relaxation ranges for the two situations.

Figure 4 summarizes all results graphically: the numerical evaluation of Eq. (50) in blue, the asymptotic expressions (81) and (73) for moderate and large κ at short times in orange, and the long-time asymptotics discussed below, see Eq. (95), in red. Starting with the simpler result (81) for moderately strong pinning $\kappa - 1 \ll 1$, we see that the increase in the curvature term in the renormalized force jump produces an increase in the Campbell curvature. The negative contribution in $\Delta f_{\rm pin}^{\rm fp, jp}$ formally dominates the curvature term only at values of the creep parameter $\mathcal{T}$ that reside beyond the criterion (82), and hence the ratio (81) increases monotonously.

At very strong pinning $\kappa \gg 1$, again, the increase in the trapping area and the curvature term in the force

jump jointly produce an increase in the Campbell curvature at small values of the creep parameter. In this rise, the curvature term is the dominant one only at very small values $\mathcal{T} < (\pi/4)^3[(4/3)^{27/4}/\sqrt{3}]\,\kappa^{-11/4}$. The curvature term goes over into the linear correction $\propto \delta x_-/x_-$ at $\mathcal{T} \approx [(2/3)^3/\sqrt{3}]\,\kappa^{-1/2}$, but this crossover is hidden by the dominant increase in the trapping area. The increasing Campbell curvature implies a decreasing Campbell length $\lambda_c \propto 1/\sqrt{\alpha_{sp}}$.

At larger values of $\mathcal{T}$, the competition is among the two $\propto \mathcal{T}^{2/3}$ terms in Eq. (73), positive and $\propto \kappa^{1/3}$ in the trapping area and negative ($\propto 1$) in the force jump, that describes an inverted parabola in $\mathcal{T}^{2/3}$. At large κ, the positive correction in the trapping area dominates and we obtain a maximum in the Campbell curvature at $\mathcal{T} \approx [(1/2)^{3/2}/\sqrt{3}](1 - 8/3\kappa^{1/3})^{3/2}$, where we have focused on the leading order in κ only. This saturates at large κ at a value $\mathcal{T} \approx 0.2$, i.e., within the relevant time range $0 < \mathcal{T} < 1$ found in (82). With decreasing κ the correction in the trapping factor diminishes and at $\kappa \sim 10$ the negative term in the force correction drives the initial slope of the inverted parabola negative, resulting in a monotonically decreasing Campbell curvature. However, we should not trust the large κ result Eq. (73) at these intermediate values of κ any more. Indeed, as shown in Fig. 4, at $\kappa = 5$, we have already crossed over from the monotonously increasing behavior predicted at marginal pinning to the nonmonotonic result typical for large values of κ.

The above results can be compared with different experimental findings: The increasing curvature α_{sp} that we find at small times produces a decreasing-in-time Campbell length $\lambda_c \propto 1/\sqrt{\alpha_{sp}}$, in agreement with experimental results on $Bi_2Sr_2CaCu_2O_8$ (BiSCCO) by Prozorov *et al.*, see Ref. [18]. On the other hand, measurements on $YBa_2Cu_3O_7$ (YBCO) by Pasquini *et al.* [19] show a Campbell length that increases with time under the effect of creep; this is consistent with our long-time decrease in α_{sp} that appears for intermediate and large values of the strong-pinning parameter κ.

In Fig. 4, we complete these results with the curves $j(t, T)$, Eq. (40), for the persistent current densities. While $j(t \to \infty, T)$ vanishes on approaching equilibrium, this is not the case for the Campbell curvature $\alpha_{sp}(t, T)$. This is due to the vanishing jumps Δe_{pin} at x_0 in the pinning energy, see Fig. 3, while the force jumps Δf_{pin} remain large at x_0 and hence $\alpha_{sp}(t \to \infty, T) \to \alpha_0$, with the latter defined in Eq. (48). The observation of a finite Campbell penetration depth above the irreversibility line [18] in a BiSCCO sample confirms this finding.

2. Long time limit $t \to t_{eq}$

On a timescale $t \to t_{eq} = t_0 \exp(U_0/T)$, the jumps $x_{\pm}^{jp}$ shift close to x_0 and the branch occupation $p_{th}(R)$ approaches the radially symmetric equilibrium distribution $p_{eq}(R)$ with a jump at $R \approx x_0$. For marginally strong pinning with $\kappa - 1 \ll 1$, the maximal barrier U_0 is small and the relaxation to equilibrium happens rapidly. The bistable region is narrow, with $x_{\pm}$ and x_0 given in Sec. II, Eqs. (16) and (24), and hence the above evaluation of the force jumps at $x_{\pm}^{jp}$ remains accurate when $x_{\pm}^{jp} \to x_0$. As shown in Fig. 4, Eq. (81) then captures the corresponding long-time limit successfully.

In the very strong pinning limit $\kappa \gg 1$, equilibrium is only slowly approached and the bistable region starts out broad and asymmetric, leading to stark changes in the trapping geometry and in the total force jump as the branch occupation relaxes. Our analysis then has to be adapted to cope with this different situation. We start by evaluating the asymptotic equilibrium value α_0, and then study how this is approached as $x_{\pm}^{jp} \to x_0$.

We simplify our previous result for α_0 at equilibrium, Eq. (48), by making use of the force balance Eq. (56) in order to express the jumps through the free and pinned tip positions at $\pm x_0$,

$$\alpha_0 = n_p \frac{\pi x_0}{a_0} \frac{\bar{C}[r_f(x_0) - r_p(x_0)]}{a_0}. \tag{83}$$

The branch cutting point x_0 has been determined in Sec. II, Eq. (23). For the Lorentzian potential, we find $x_0 \approx 2\sqrt{2\kappa}\,\xi$. Combining Eq. (83) with the results for x_0 and the associated tip positions $r_f(x_0) \approx x_0$ and $r_p(x_0) \ll \xi$, see Eq. (22), we arrive at the result

$$\alpha_0 \approx 2\pi\, n_p\,(e_p/a_0^2) \tag{84}$$

that depends only on the defect density n_p and depth e_p. Quite remarkably, while the persistent current density vanishes upon approaching equilibrium, the Campbell curvature and penetration depth remain finite. This is in agreement with the experimental findings in Ref. [18], where a finite Campbell length was observed above the irreversibility line in a BiSCCO sample.

On approaching equilibrium, the thermal jumps reside close to x_0 and we can write $x_{\pm}^{jp} = x_0 \pm \delta x_{0\pm}$ with small corrections $\delta x_{0\pm} > 0$. Using the general result Eq. (50) for the Campbell curvature with $\theta_+^{jp} \approx \pi$, see Eq. (46) and making use of the smallness of $\delta x_{0\pm}$, we have to evaluate

$$\alpha_{sp}(t, T) = n_p \frac{\pi}{2}\left[\frac{(x_0 + \delta x_{0+})}{a_0}\frac{\Delta f_{pin}^{fp,jp}}{a_0}\right.$$
$$\left. + \frac{(x_0 - \delta x_{0-})}{a_0}\frac{\Delta f_{pin}^{pf,jp}}{a_0}\right]. \tag{85}$$

With $f_{pin}^f(x) \approx 0$ and $f_{pin}^p(x) \approx -\bar{C}x$ in the vicinity of x_0, we find the changes in the force jump away from x_0

$$\Delta f_{pin}^{fp,jp} - \Delta f_{pin}^{fp}(x_0) \approx \bar{C}\delta x_{0+}, \tag{86}$$

$$\Delta f_{pin}^{pf,jp} - \Delta f_{pin}^{fp}(x_0) \approx -\bar{C}\delta x_{0-}. \tag{87}$$

For long times $t \to t_{eq}$, the relevant creep barriers (35) are to be evaluated close to the equilibrium value U_0, justifying the expansions

$$U_{dp}(x_+^{jp}) \approx U_0 + U'_{dp}(x_0)\,\delta x_{0+}, \tag{88}$$

$$U_p(-x_-^{jp}) \approx U_0 + U'_p(-x_0)\,\delta x_{0-}, \tag{89}$$

with the total derivatives assuming the simple form

$$U'_p(-x_0) \approx \bar{C}(r_{us} - r_f)|_{x_0} < 0, \tag{90}$$

$$U'_{dp}(x_0) \approx \bar{C}(r_p - r_{us})|_{x_0} < 0, \tag{91}$$

as all derivatives $\partial_x r_f(x)$ and $\partial_x r_{us}(x)$ cancel due to Eq. (56); indeed, both barriers decrease when going away from equilibrium. Combining the above relations, we can express the change in the force jumps $\Delta f_{pin}^{dp,jp}$ and $\Delta f_{pin}^{pf,jp}$ in terms of the barrier difference

$$U_0 - U = T \ln(t_{eq}/t) \equiv e_p \mathcal{T}_{eq} \tag{92}$$

to find

$$\Delta f_{pin}^{fp,jp}(t,T) - \Delta f_{pin}^{fp}(x_0) \approx \frac{e_p}{r_{us} - r_p} \mathcal{T}_{eq}, \tag{93}$$

$$\Delta f_{pin}^{fp,jp}(t,T) - \Delta f_{pin}^{fp}(x_0) \approx -\frac{e_p}{r_f - r_{us}} \mathcal{T}_{eq}. \tag{94}$$

Combining Eqs. (86) and (93) also provides us with the expressions for $\delta x_{0\pm}$ that we need in (85). As a result, we have reduced the problem to the determination of the three vortex tip positions $r_i(x_0)$, i = p, us, f, at the asymptotic vortex position x_0. These have been found in Sec. II, Eqs. (22) and (26).

Inserting the results for the force jumps and jump points into Eq. (85) and focusing on a Lorentzian potential, we find the scaled Campbell curvature near equilibrium,

$$\frac{\alpha_{sp}(t,T)}{\alpha_0} \approx \frac{(1 - \mathcal{T}_{eq}/2)^2 + (1 + (\kappa/2)^{1/3} \mathcal{T}_{eq})^2}{2}, \tag{95}$$

where we have used the form (48) for α_0 with $\Delta f_{pin}^{fp}(x_0) \approx 2\bar{C}(2\kappa)^{1/2}\xi$ and $x_0 \approx 2\sqrt{2\kappa}\,\xi$. Again, we find a competition between the trapping length and the force jump that act the same way as before, with the opposite signs compensated by evaluating $\mathcal{T}_{eq}$ away from the longest time $t_{eq} = t_0 \exp(U_0/T)$. The result is shown in the large κ panel of Fig. 4 and agrees well with the full numerical result close to equilibrium, where $\delta x_{0\pm}/x_0 \ll 1$.

Going to very large times $t > t_{eq}$, we enter the TAFF regime [28] with a diffusive vortex motion characterized by the TAFF resistivity, $\rho_{TAFF} \propto \rho_{flow} \exp(-U_0/T)$ and $\rho_{flow} = (B/H_{c2})\rho_n$, cf. the corresponding discussion of the asymptotic decay of the persistent current density $j(t,T)$ in Sec. III B above. The penetration of the magnetic field then changes its nature from the Campbell response characterized by λ_c to the skin-effect with the frequency dependent penetration depth $\lambda_{TAFF}(\omega) = \sqrt{c^2\rho_{TAFF}/2\pi\omega}$: In the Campbell regime, vortices displace by $U \sim jB/\alpha c$ at frequency ω, resulting in a typical velocity $v_c \sim \omega U \sim (4\pi\omega\lambda_c^2/Bc)\,j$. The typical velocity due to the dissipative motion follows from Faraday's law, $E = vB/c$, combined with Ohm's law $E = \rho_{TAFF}j$, hence $v_{TAFF} \sim (c\rho_{TAFF}/B)\,j$. Equating the two velocities, $v_c = v_{TAFF}$, we find the crossover frequency $\omega_{TAFF} = c^2\rho_{TAFF}/4\pi\lambda_c^2$, where $\lambda_c \sim \lambda_{TAFF}$. We then enter the skin-effect regime at low frequencies $\omega < \omega_{TAFF}$ where the response involves both an exponential and an oscillatory component,

$$\delta B = h_{ac} e^{-X/\lambda_{TAFF}} e^{i(X/\lambda_{TAFF} - \omega t)}, \tag{96}$$

see Refs. [31,32] for a detailed discussion. Physically, as v_c drops below v_{TAFF}, the ac oscillation of the vortex in the well is prematurely (i.e., before completion of one cycle) terminated by an escape out of the well.

Note that the Campbell response requires sufficiently small frequencies as well. Following the derivation of Eq. (41), the Campbell penetration physics requires frequencies $\omega < \alpha/\eta$ that transforms to the condition $\omega < \omega_{flow}$ with $\omega_{flow} = c^2\rho_{flow}/4\pi\lambda_c^2$. As a result, we find the bounded regime $\omega_{TAFF} < \omega < \omega_{flow}$ for the application of the Campbell response at very long times $t > t_{eq}$, with a crossover to the usual skin effect [with $\rho = \rho_{TAFF} \propto \rho_{flow} \exp(-U_0/T)$] at very low and at very high frequencies (with $\rho = \rho_{flow}$).

C. Campbell penetration depth λ_c in FC state

The FC state is characterized by a homogeneous distribution of the magnetic field inside the sample and hence is associated with a vanishing current- and pinning-force density. Correspondingly, at $\kappa > 1$, the branch occupation $p_{FC}(R)$ is rotationally symmetric assuming a value $p_{FC} \approx 1$ in a disk with radius $x^{jp} \in [x_-, x_+]$ centered around the defect (we note that in Ref. [12], the trapping area for λ_c was handled the same way as for j_c; it was described by the transverse trapping length $t_\perp = 2x_- \sim 2\xi$ and its circular geometry was ignored). The determination of the jump position x^{jp} as a function of the FC state preparation and its relaxation through creep is the main objective of this section.

Ignoring the initialization process [29], as we did in the discussion of the ZFC case above, we determine the restoring force $\delta F_{pin}(U)$ using Eq. (42) with $p_c(R)$ replaced by $p_{FC}(R) = \Theta(x^{jp} - R)$; accounting for the radial symmetry of the problem, we find the restoring force density

$$\delta F_{pin}(U) \approx -n_p \frac{\pi x^{jp}}{a_0} \frac{\Delta f_{pin}^{fp}(x^{jp})}{a_0} U, \tag{97}$$

directed along the displacement **U** parallel to the x-axis, $\mathbf{U} = (U, 0)$; the force jump $\Delta f_{pin}^{fp}(x^{jp}) = f_{pin}^f(x^{jp}) - f_{pin}^p(x^{jp})$ is to be evaluated at the radial jump position x^{jp}. The Campbell curvature then reads

$$\alpha_{sp}^{FC} = n_p \frac{\pi x^{jp}}{a_0} \frac{\Delta f_{pin}^{fp}(x^{jp})}{a_0} \tag{98}$$

and depends on temperature through the position of the jump x^{jp} in multiple ways: first, the pinning parameter κ determining the shape of the pinning force landscape $f_{pin}(x)$ in Fig. 3 depends on T and B through the parameters of the mean-field Ginzburg-Landau theory which are functions of $(1 - T/T_c)$ and $(1 - T/T_c - B/H_{c2(0)})$ with H_{c2} the upper critical field [12]—this dependence generates interesting hysteretic phenomena in cyclic measurements of the Campbell penetration depth with varying temperature T [9,12] $\lambda_c(T)$ and will be the subject of Sec. IV C 1. Second, thermal fluctuations, i.e., creep, drive the vortex state towards equilibrium, that corresponds to a relaxation of the initial jump position x^{jp} after field cooling towards the equilibrium position x_0 characterizing p_{eq}—these creep phenomena associated with the relaxing FC state will be discussed in Sec. IV D.

1. Hysteresis of penetration depth λ_c in FC state

We start with the discussion of the field-cooled state and the appearance of hysteretic effects. Here, we have in mind a setup where we fix the magnetic field H and vary the temperature T, typically in a (repeated) cooling-warming cycle. By changing the temperature T, the vortex lattice elastic constant $\bar{C}$ and the pinning energy e_p are modified

through their dependence on the Ginzburg-Landau parameters $\lambda(T, B) \propto (1 - \tau - b_0)^{-1/2}$ and $\xi(T) \propto (1 - \tau)^{-1/2}$ on the reduced temperature $\tau = T/T_c$ and reduced field $b_0 = B/H_{c2}(0)$ (we ignore rounding effects appearing at small temperatures). These mean-field dependencies on T and B entail a change in the pinning parameter κ within the B-T phase diagram that varies with the nature of the defect,

$$\kappa(\tau, b_0) \sim \frac{k}{\sqrt{b_0}} (1 - \tau)^{\alpha} (1 - \tau - b_0)^{\beta}, \qquad (99)$$

with the prefactor k and exponents α and β depending on the type of defect/pinning (the dependence $\propto 1/\sqrt{b_0}$ derives from the field dependence in the effective elasticity; at very small fields, we enter the single vortex strong pinning regime where our analysis has to be adapted, see Ref. [8]). The cases of small insulating ($k = (\rho/\xi_0)^3, \alpha = 3/2, \beta = 1/2$) or metallic defects ($k = 1, \alpha = 0, \beta = 1/2$), of δT_c-pinning (with local changes δT_c in the transition temperature T_c and $k = (\rho/\xi_0)^3 (\delta T_c / T_c), \alpha = 3/2, \beta = -1/2$) or $\delta \ell$-pinning (with local changes $\delta \ell$ in the mean free path ℓ and $k = (\rho/\xi_0)^3 (\delta \ell / \ell)$, $\alpha = 5/2, \beta = -1/2$) have been discussed in Ref. [12], but other situations may produce alternative dependencies (here, ρ is the size of the defect and ξ_0 the coherence length of the superconducting material at $T = 0$). Depending on the type of defect, strong pinning may turn on smoothly at the phase boundary $H_{c2}(T)$ (this is the case for insulating and metallic defects with $\beta > 0$) or collapse from infinity (this is the case for δT_c- and $\delta \ell$-pinning with $\beta < 0$). However, owed to the factor $(1 - \tau)^{\alpha}$ with a large exponent $\alpha = 3/2, 5/2$ characterizing δT_c- and $\delta \ell$-pinning, this divergence at $H_{c2}(T)$ is strongly suppressed at the small fields where our analysis is valid. As a result, at small fields, strong pinning always turns on smoothly upon decreasing the temperature T below the phase boundary $T_{c2}(H)$. Also note that thermal fluctuations near the transition shift the onset of pinning to below $T_{c2}(H)$.

In a first step, we establish the onset of strong pinning upon decreasing the temperature T below $T_{c2}(H)$ at a given field value H. Figure 5 shows the pinning force profile $f_{\text{pin}}(x)$ at the onset of strong pinning where the function $f_{\text{pin}}(x)$ develops an infinite slope at the point x_{0L}. This happens at the Labusch temperature T_L that is defined through the condition $\kappa(T_L) = 1$. The point x_{0L} corresponds to the asymptotic position x_m associated with the inflection point r_m of $f_p(r)$ at the Labusch point $\kappa = 1$, hence $x_{0L} = x_m = r_m - f_p(r_m)/\bar{C}$ with $f_p''(r_m) = 0$ and $f_p'(r_m) = \bar{C}$, as discussed in Sec. II, Eqs. (13) and (18). At $\kappa \to 1$, this point coincides with the branch crossing point x_0, see Eq. (24).

Decreasing the temperature T below T_L, the singularity at x_{0L} develops into the finite bistable interval $[x_-, x_+]$ with a width $x_+ - x_- \sim (\kappa - 1)^{3/2} \xi$ initially centered around $x_0 \approx (x_+ + x_-)/2 \sim [\text{const.} + (\kappa - 1)]\xi$. Depending on the relative increase in $\kappa(\tau)$ and the decrease in $\xi(\tau) \approx \xi_0/\sqrt{1 - \tau}$, the bistable interval may grow to the right (or left) of x_{0L} with $x_{0L} < x_-$ ($x_{0L} > x_+$) or enclose the initial instability at x_{0L} with $x_- < x_{0L} < x_+$. Going to smaller temperatures, pinning becomes stronger and the bistable interval $[x_- \sim \kappa^{1/4}\xi, x_+ \sim \kappa\xi]$ increases asymmetrically around $x_0 \sim \sqrt{\kappa}\xi$; again, the competition between the growing $\kappa(\tau)$ and the decreasing
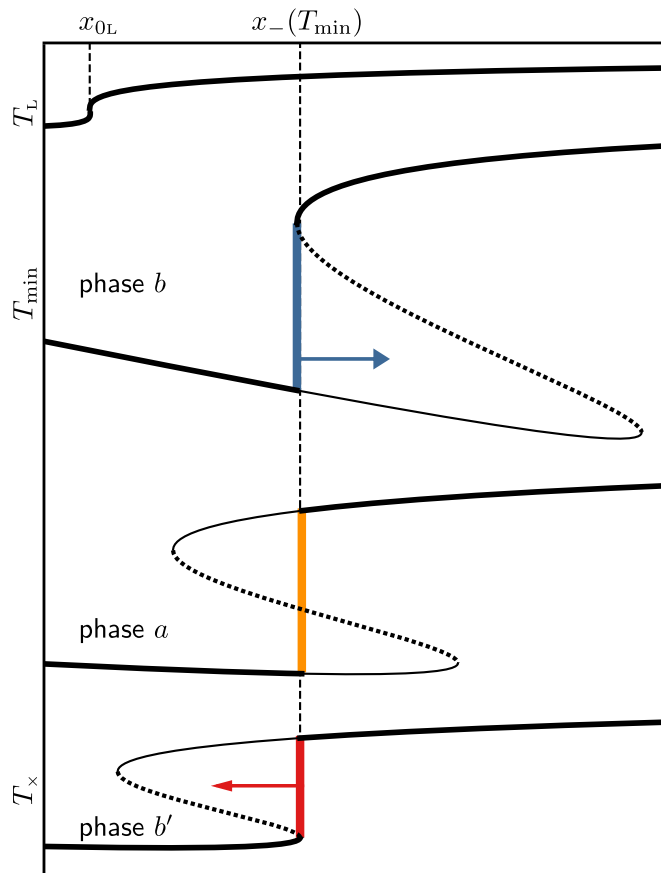

FIG. 5. Illustration of the evolution of the force profile $f_{\text{pin}}(x)$ and of the branch occupation along a temperature cycle $T_L \to T_{\text{min}} \to T_L$. Top curve: strong pinning turns on at the Labusch temperature T_L where $\kappa(T_L) = 1$, with an infinite slope in $f_{\text{pin}}(x)$ appearing at x_{0L}. Lowering the temperature $T < T_L$, a bistable region opens up, widens, and moves with respect to first instability point x_{0L}. Shown here is the case for an insulating defect (or $\delta \ell$-pinning), where the bistable interval moves to the right/left upon cooling/heating. Bottom three curves: the three phases b (cooling), a (heating), and b' (heating) of the hysteresis loop are characterized by different branch occupations with jump positions within $f_{\text{pin}}(x)$ marked in blue, orange, and red. Upon cooling below T_L, the branch occupation (thick solid line) changes as parts of the force profile become unstable. The jump x^{jp} in the branch occupation first follows the inner endpoint (phase b), $x_b^{\text{jp}}(T) = x_-(T)$ (blue solid line, drawn at T_{min}). Reversing the change in temperature at T_{min}, the bistable region shrinks while heating and moves leftwards, leaving the jump position $x^{\text{jp}}(T)$ unchanged, $x_a^{\text{jp}} = x_-(T_{\text{min}})$ (orange solid line in phase a). When reaching the right end of the S-shaped force-profile at the crossover temperature $T_\times$, $x_+(T_\times) = x_a^{\text{jp}}$, the jump point gets pinned to the boundary x_+ of the bistable region, $x_{b'}^{\text{jp}}(T) = x_+(T)$ (red solid line in phase b', drawn at $T_\times$). If at some temperature T the cycle is interrupted, the vortex lattice relaxes towards equilibrium with $x_{b,b'}^{\text{jp}}(T) \to x_0(T)$, as indicated by the horizontal arrows in phases b and b'. In the intermediate phase a, relaxation is weak and depends on the relative position between $x_a^{\text{jp}}(T)$ and the edges $x_\pm(T)$.

$\xi(\tau)$ determines the evolution of the bistable interval with decreasing temperature.

Depending on which of the above scenarios is realized, the system will exhibit quite a different behavior. To fix ideas,
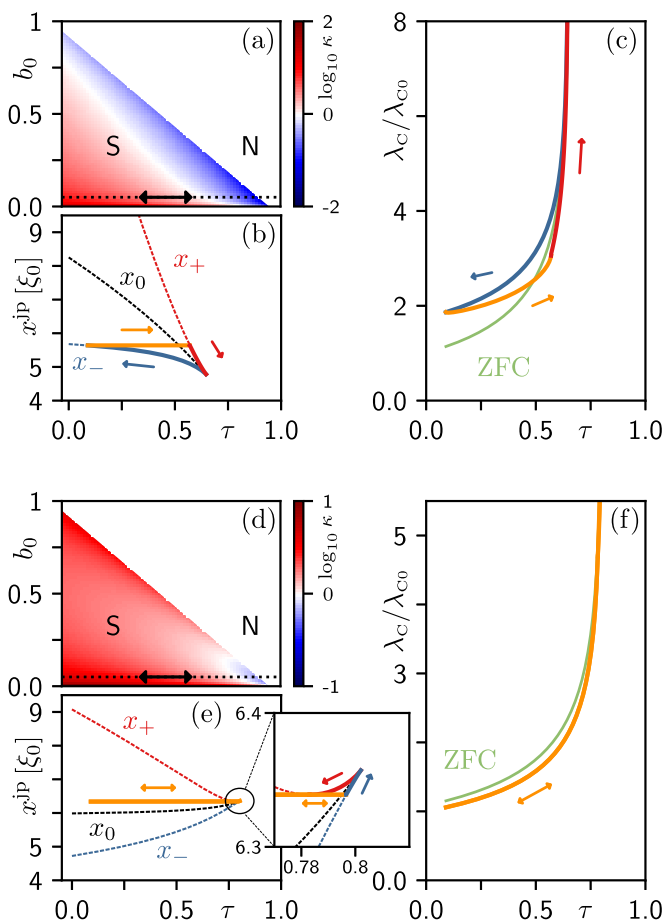
FIG. 6. Characteristics of strong pinning for insulating defects (top, relative defect size $\rho/\xi_0 = 1.25$) and for δT_c pinning (bottom, same ratio ρ/ξ_0 and $\delta T_c/T_c = 0.5$) assuming a Lorentzian potential. [(a) and (d)] show maps of the pinning parameter κ over the b_0–τ phase diagram (N and S denote normal and superconducting phases); we focus on small fields $b_0 = 0.05$, with strong pinning (red) turning on at $\kappa = 1$ (white color) when decreasing temperature. [(b) and (e)] Evolution of the edges x_+ (red dots) and x_- (blue dots) of the bistable pinning region, as well as branch crossing point x_0 (black dots), with decreasing temperature τ. During a cooling-warming cycle, the jump position x^{jp} follows the phases b (blue line), a (orange), b' (red) in (b) but remains fixed in the a phase (orange) near $x_{0\mathrm{L}}$ except for a small region near the strong-pinning onset, see (e) and expanding inset. [(c) and (f)] Hysteretic trace of the Campbell length $\lambda_{\mathrm{C}}(\tau)$ for a cooling-warming cycle, normalized with respect to $\lambda_{\mathrm{C0}} = (B_0^2/4\pi\alpha_0)^{1/2}$, α_0 the equilibrium Campbell curvature at $T = 0$. Colors indicate different phases a (orange), b (blue), and b' (red) assumed along the cooling-warming cycle; the ZFC trace (green) is shown for comparison. Insulating defects produce a hysteretic trace with x^{jp} following x_- on cooling that is changing over via the a phase to x_+ on heating, see (b). For δT_c-pinning, no memory effect shows up away from the Labusch point, that is owed to the fixed jump position $x^{\mathrm{jp}} \approx x_{0\mathrm{L}}$ in (e).

let us start with the specific case of an insulating defect with $\alpha = 3/2$, $\beta = 1/2$ and a small field b_0; the evolution of the Labusch parameter $\kappa(\tau, b_0)$ within the B-T phase diagram is shown in Fig. 6(a). Decreasing T below T_{L}, one finds that the slope $\partial_\tau x_\pm|_{T_{\mathrm{L}}} < 0$ and hence the bistable interval

$[x_-, x_+]$ moves to larger values of x, $x_{0\mathrm{L}} < x_- < x_+$. Going to smaller temperatures with larger values of κ, one finds that $x_- \sim$ const. and $x_+ \propto (1 - \tau)^{3/2}$ increases with decreasing temperature, hence the interval $[x_-, x_+]$ continues shifting to the right as T goes down, see Fig. 6(b).

This is the situation illustrated in Fig. 5: With parts of the S-shaped force profile $f_{\mathrm{pin}}(x)$ turning unstable, the jump position x^{jp}, starting out at $x_{0\mathrm{L}}$, gets pinned to the left (pinning) edge of the S-profile, $x_b^{\mathrm{jp}}(T) = x_-(T)$—we name this the phase b. This behavior continues until the further decrease in temperature is stopped at the minimal temperature T_{min} of the cycle where x^{jp} reaches its maximal value $x_b^{\mathrm{jp}}(T_{\mathrm{min}})$. Upon raising the temperature, we enter phase a of the cycle where the bistable region shrinks and moves leftward; the jump position then stays fixed at its maximum, $x_a^{\mathrm{jp}} = x_-(T_{\mathrm{min}})$ until the right end $x_+(T)$ of the bistable region coincides with the jump at x_a^{jp} at the crossover temperature $T_\times$, $x_-(T_{\mathrm{min}}) = x_+(T_\times)$. From $T_\times$ onwards, the jump position is pinned to the right edge of the S-profile, with $x_{b'}^{\mathrm{jp}}(T) = x_+(T)$; this is denoted as phase b' in Fig. 5. The complete hysteretic loop traced out by $x^{\mathrm{jp}}(T)$ over the three phases b, a, and b' is shown in Fig. 6(b). Finally, the changeover between phases b, a, and b' produces a pronounced hysteresis in the Campbell penetration depth $\lambda_{\mathrm{C}}(\tau)$, as illustrated in Fig. 6(c).

Having established the cycle $T_{\mathrm{L}} \to T_{\mathrm{min}} \to T_\times \to T_{\mathrm{L}}$ for the insulating defect, let us briefly discuss other possibilities. Another typical situation is shown in Figs. 6(d)–6(f), where we show the Labusch parameter $\kappa(\tau, b)$ for the case of δT_c-pinning in (d), together with the evolution of x_-, x_+, and x_0 as well as the resulting cycle in (e), and the Campbell penetration depth $\lambda_{\mathrm{C}}(\tau)$ in (f). In this case, we find that $\partial_\tau x_\pm|_{T_{\mathrm{L}}} > 0$, hence the S shaped instability in $f_{\mathrm{pin}}(x)$ initially moves to the left, $[x_-, x_+] < x_{0\mathrm{L}}$. However, as shown in Fig. 6(e) and the expanded box, the upper edge x_+ quickly turns around with further decreasing T and we change over from a narrow b' phase to an a phase that completely dominates the cycle. With the jump $x^{\mathrm{jp}}(\tau)$ remaining fixed close to $x_{0\mathrm{L}}$ deep in the bistable regime over the entire cycle, we find essentially no hysteresis for the case of δT_c pinning, except for a narrow region close to T_{L}.

The two other cases, $\delta\ell$ pinning (with $\partial_\tau x_\pm|_{T_{\mathrm{L}}} < 0$) and the metallic defect (with $\partial_\tau x_\pm|_{T_{\mathrm{L}}} = 0$) closely resemble the behavior of the insulating defect and of δT_c pinning, respectively, see Fig. 7, with an important difference remaining, though. Indeed, focusing on the metallic defect and the δT_c-pinning, with both not developing a hysteresis, we notice that for δT_c-pinning the a phase is realized deep in the bistable interval with $x^{\mathrm{jp}}(\tau)$ far away from the edges $x_\pm(\tau)$, while for the metallic defect, the a phase resides close to the edge with $x^{\mathrm{jp}}(\tau) \approx x_+(\tau)$, i.e., close to phase b'. As we have already learnt in Sec. IV B, creep is strong when the barriers are small, which is the case when the jumps at x^{jp} are close to the edges $x_\pm$, see Fig. 3. On the other hand, creep is weak when the jump x^{jp} resides deep within the bistable interval, e.g., away from the edges $x_\pm(T)$ where barriers become large. Hence, we conclude that creep is strong in phases b and b' where the jump x^{jp} is pinned to the edges, but is weak, deep in the phase a. And hence, we expect that for δT_c-pinning creep will be small, while the metallic defect will exhibit stronger creep.
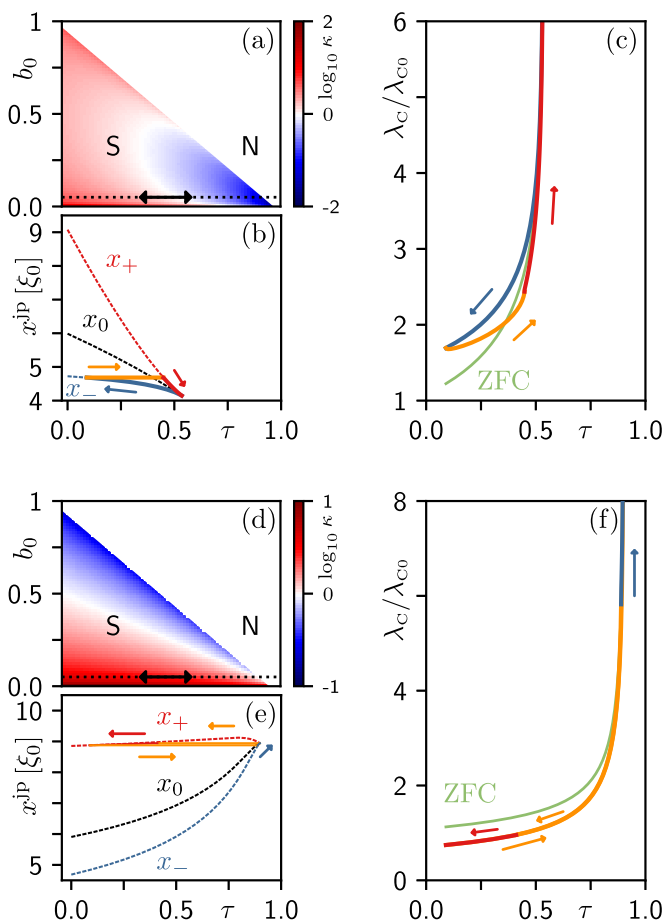
FIG. 7. Characteristics of strong pinning for $\delta\ell$ pinning (top, with $\delta\ell/\ell = 0.5$) and for metallic defects (bottom) assuming a Lorentzian potential. [(a) and (d)] show maps of the pinning parameter κ over the b_0–τ phase diagram (N and S denote normal and superconducting phases); we focus on small fields $b_0 = 0.05$, with strong pinning (red) turning on below $\kappa = 1$ (white color) when decreasing temperature. [(b) and (e)] Evolution of the edges x_+ (red dots) and x_- (blue dots) of the bistable pinning region, as well as branch crossing point x_0, with decreasing temperature τ. During a cooling-warming cycle, the jump position x^{jp} follows the phases b (blue line), a (orange), and b' (red) in (b) but remains close to x_{0L} and x_+ in (e), following a thin cycle a (orange), b' (red), a (orange), and b (blue). [(c) and (f)] Hysteretic trace of the normalized Campbell length $\lambda_C(\tau)$ for a cooling-warming cycle. Colors indicate different phases a (orange), b (blue), and b' (red) assumed along the cooling-warming cycle; the ZFC trace (green) is shown for comparison. $\delta\ell$ pinning produces a hysteretic trace with x^{jp} following x_- on cooling that is changing over via the a phase to x_+ on heating, see (b). For metallic defects, memory effects are small, see (e) and (f), as the jump point always remains close to x_{0L} and x_+.

We thus conclude, that 'reading' a temperature cycle of the Campbell penetration depth $\lambda_C(\tau)$ allows us to gain quite some insights into the pinning mechanism.

For an insulating defect and for $\delta\ell$ pinning, the cycle is hysteretic with strong creep upon cooling in the b phase, weak creep upon heating in the a phase, and again strong creep in the final heating phase close to T_L where the b' phase is realized. For a metallic defect, the cycle is nonhysteretic but creep

is reasonably strong since the system straddles the regime at the edge of the a phase/b' phase. Finally, for δT_c pinning, the cycle is again nonhysteretic but with weak creep as the system resides deep in the a phase. We note, that other pinning types may occur exhibiting cycles that are yet different from those analyzed here.

Below, we determine the Campbell curvatures α_{sp}^{FC} for the different phases a, b, and b'. These results then produce the Campbell penetration depth $\lambda_C(\tau)$ shown in Figs. 6(c) and 6(f) and 7(c) and 7(f). While for the b and b' phases the jump positions at the edges $x_\pm$ are well defined, for the a phase the jump position depends on the way the phase is entered. For example, for the cooling-warming loop with underlying insulating defects or with $\delta\ell$-pinning, we have $x_a^{jp} = x_-(T_{min})$ since we enter the a phase from the b phase, while for metallic defects, we enter the a phase upon the onset of strong pinning and hence $x_a^{jp} = x_{0L}$. In a third case, realized for $\delta\ell$-pinning, the a phase is entered through the b' phase with $x_a^{jp} = x_+(T_{inf})$ and T_{inf} the temperature where $\partial_\tau x_+(\tau)$ changes sign; this situation is realized for δT_c-pinning close to T_L, see Fig. 6(e). All these different cases produce different values for x_a^{jp}.

2. Campbell curvatures for FC phases

We now determine the Campbell curvatures α_{sp}^{FC} for the different phases a, b, and b' potentially appearing in a hysteresis loop, first in the marginal strong pinning situation $\kappa - 1 \ll 1$ valid close to T_L and thereafter at large κ potentially realized at small temperatures. For convenience, we scale the results for the curvatures α_{sp}^{FC} using the corresponding ZFC results α_{sp}, where we denote field-cooled results via an upper index ^{FC} or with specific phase indices $^{a,b,b'}$, while the ZFC expressions remain without upper index. Furthermore, while the results for the b and b' phases can be pushed to closed expressions, this is not the case for the a phase, as for the latter the jump position x_a^{jp}, while constant in temperature, resides somewhere within the bistable interval $[x_-, x_+]$, as discussed above.

Let us start close to the Labusch point $\kappa - 1 \ll 1$ where the ZFC result for the Campbell curvature follows from Eq. (47) with the trapping scale x_0 and the force jump (80), providing the result

$$\alpha_{sp} \approx \frac{3\pi x_0 \xi}{a_0^2} \left(\frac{4\bar{C}\xi^2}{e_p}\right)^{1/2} \left(\frac{\kappa - 1}{4\gamma}\right)^{1/2} n_p \bar{C}. \quad (100)$$

For the Lorentzian-shaped potential, this reduces to the simple expression $\alpha_{sp} \approx \sqrt{3\pi}\sqrt{\kappa - 1}\, n_p\, (e_p/a_0^2)$, where we have used that $x_0 \approx 2\sqrt{2}\xi$ to leading order in $\kappa - 1$.

For the FC state at marginal pinning $\kappa - 1 \ll 1$, we evaluate the Campbell curvature (98) using the jump radius x_0 that is same to leading order in $\kappa - 1$ for all three phases a, b, b'. We find the force jumps with the help of the force balance equation (56), $\Delta f_{pin}^{fp}(x) = \bar{C}[r_f(x) - r_p(x)]$, and make use of Eqs. (14) and (21) for the tip positions at the characteristic points $x_\pm$ relevant in phase b and b' of the cycle. Furthermore, at small values $\kappa - 1 \ll 1$, the bistable interval is narrow and symmetric around x_0; we then choose $x_a^{jp} = x_0$ as a represen-

tative point (with the largest force jump) and make use of

$$r_{\mathrm{f}}(x_0) - r_m = -r_{\mathrm{p}}(x_0) + r_m \approx \sqrt{\frac{3\bar{C}\xi^4}{\gamma e_p}}(\kappa - 1)^{1/2}. \quad (101)$$

As a result, we find the force jumps,

$$\Delta f_{\mathrm{pin}}^{\mathrm{fp}}(x_{\pm}) \approx \frac{3}{2}\bar{C}\xi\sqrt{\frac{4\bar{C}\xi^2}{\gamma e_p}}(\kappa - 1)^{1/2}, \quad (102)$$

$$\Delta f_{\mathrm{pin}}^{\mathrm{fp}}(x_0) \approx \sqrt{3}\bar{C}\xi\sqrt{\frac{4\bar{C}\xi^2}{\gamma e_p}}(\kappa - 1)^{1/2}, \quad (103)$$

relevant, respectively, for the b, b', and a phases of the temperature cycle. For a Lorentzian potential, $\gamma = 3/8$ provides the force jumps $\Delta f_{\mathrm{pin}}^{\mathrm{fp}}(x_{\pm}) \approx [\sqrt{3/8}\,(\kappa - 1)^{1/2}]e_p/\xi$ and $\Delta f_{\mathrm{pin}}^{\mathrm{fp}}(x_0) \approx [(\kappa - 1)^{1/2}/\sqrt{2}]e_p/\xi$. Inserting these results in the expression (98) for the Campbell curvature, we find, to leading order in $\kappa - 1$,

$$\alpha_{\mathrm{sp}}^{b,b'} \approx \sqrt{3}\pi(\kappa - 1)^{1/2}n_p(e_p/a_0^2), \quad (104)$$

$$\alpha_{\mathrm{sp}}^{a} \approx 2\pi(\kappa - 1)^{1/2}n_p(e_p/a_0^2). \quad (105)$$

Finally, comparing the FC and ZFC results, we obtain the ratios

$$\frac{\alpha_{\mathrm{sp}}^{b,b'}}{\alpha_{\mathrm{sp}}} \approx 1 \quad \text{and} \quad \frac{\alpha_{\mathrm{sp}}^{a}}{\alpha_{\mathrm{sp}}} \approx \frac{2}{\sqrt{3}} \approx 1.15 \quad (106)$$

valid in the vicinity of the Labusch temperature $T \lesssim T_{\mathrm{L}}$. Given the symmetry between x_- and x_+ of the bistable region within the marginally strong pinning limit, the force jumps in the b and b' phases are equal to the force jump (80) in the ZFC state, and hence the FC Campbell curvature is identical to the ZFC result in the limit $\kappa \to 1$. For the representative point $x_a^{\mathrm{jp}} = x_0$ in the a phase, the force jump is larger by a factor $2/\sqrt{3} \approx 1.15$, resulting in a larger ratio for the Campbell curvature.

Including the next (fourth) order term $\tau(e_p/4\xi^5)\,\delta r^4$ in the expansion (13) for $f_p(r_m + \delta r)$, we find an asymmetric correction to $\delta r_{\max}$ in Eq. (15),

$$\delta r_{\max}(x_{\pm}) \approx \delta r_{\max} \mp \frac{\xi}{8}\frac{\tau}{\gamma^2}\frac{4\bar{C}\xi^2}{e_p}(\kappa - 1), \quad (107)$$

where the indices $\pm$ refer to pinned and free branches, respectively. For a Lorentzian potential, we have $\tau = 15/(24\sqrt{2})$. Accounting for these 4th order corrections in the evaluation of the force jumps (102), the results $\alpha_{\mathrm{sp}}^{b,b'}$ for the b and b' phases separate, in fact, symmetrically with respect to the ZFC result, $\alpha_{\mathrm{sp}}(t) = [\alpha_{\mathrm{sp}}^{b}(t) + \alpha_{\mathrm{sp}}^{b'}(t)]/2$, as the latter involves jumps both at x_+ and x_-. In Fig. 9, we show our analytic results for $\alpha_{\mathrm{sp}}^{b,b'}$ at marginally strong pinning and find that they compare well with the numerical results in the limit $t \to t_0$ discussed here.

At smaller temperatures, the pinning parameter κ grows larger and the Campbell curvature has to be evaluated in the $\kappa \gg 1$ limit. Using the expressions (8)–(10) for the endpoints x_+ and x_-, we find that the Campbell curvature in the ZFC state scales as

$$\alpha_{\mathrm{sp}} \approx n_p\frac{2x_-}{a_0}\frac{\bar{C}x_+}{a_0} \sim n_p\kappa^{1/(n+2)}(e_p/a_0^2) \quad (108)$$

for an algebraically decaying potential and $\alpha_{\mathrm{sp}} \approx \sqrt{6}\,(3\kappa)^{1/4}n_p\,(e_p/a_0^2)$ for the Lorentzian. For the FC state, we approximate the relevant force jumps in the phases a, b, and b' as [cf. Eq. (10)]

$$\Delta f_{\mathrm{pin}}^{\mathrm{fp}}(x_a^{\mathrm{jp}}) \approx \bar{C}r_{\mathrm{f}}(x_a^{\mathrm{jp}}) \approx \bar{C}x_a^{\mathrm{jp}},$$

$$\Delta f_{\mathrm{pin}}^{\mathrm{fp}}(x_-) \approx \bar{C}r_{\mathrm{f}}(x_-) \approx \frac{n+1}{n+2}\bar{C}x_-, \quad (109)$$

$$\Delta f_{\mathrm{pin}}^{\mathrm{fp}}(x_+) \approx \bar{C}x_+,$$

with x_a^{jp} depending on the specific situation, see the discussion above. We then arrive at the following results for the curvatures in phases a, b, and b' of the hysteretic temperature cycle,

$$\alpha_{\mathrm{sp}}^{a} \approx \pi\left(\frac{x_a^{\mathrm{jp}}}{a_0}\right)^2 n_p\bar{C},$$

$$\alpha_{\mathrm{sp}}^{b} \approx \pi\frac{n+1}{n+2}\left(\frac{x_-}{a_0}\right)^2 n_p\bar{C}, \quad (110)$$

$$\alpha_{\mathrm{sp}}^{b'} \approx \pi\left(\frac{x_+}{a_0}\right)^2 n_p\bar{C}.$$

Making use of the large-κ expressions (11) and (12) for $x_{\pm}$ and focusing on a Lorentzian potential, we find

$$\alpha_{\mathrm{sp}}^{b} \approx (16/3\kappa)^{1/2}\pi\,n_p(e_p/a_0^2), \quad (111)$$

$$\alpha_{\mathrm{sp}}^{b'} \approx (3/2)^3(\kappa/4)\pi\,n_p(e_p/a_0^2), \quad (112)$$

resulting in the following ratios valid at large κ

$$\frac{\alpha_{\mathrm{sp}}^{b}}{\alpha_{\mathrm{sp}}} \approx 2\sqrt{\frac{2}{3}}\frac{\pi}{(3\kappa)^{3/4}}, \quad (113)$$

$$\frac{\alpha_{\mathrm{sp}}^{b'}}{\alpha_{\mathrm{sp}}} \approx \frac{3}{32}\sqrt{\frac{3}{2}}(3\kappa)^{3/4}\pi. \quad (114)$$

The expression in (110) for the a phase cannot be brought to a simpler closed form as x_a^{jp} depends on the preparation. The above results differ from those in Ref. [12] due to the more accurate handling of the (circular) trapping geometry in the FC situation. At small temperatures and large κ, the equivalence between the Campbell curvature in the phases b and b' is broken, and the corresponding results are substantially different from the ZFC ones, a consequence of the asymmetric nature of the bistable region at large κ. Note the result (114) that turns out large; the scaling $\propto \kappa^{3/4}$ follows from the different trapping areas, $x_+^2 \propto \kappa^2$ for the FC case and $x_+x_- \propto \kappa\kappa^{1/4}$ for the ZFC state.

In Figs. 6(c), 6(f) and 7(c), 7(f) we translate the curvatures α^{FC} to the Campbell penetration depth $\lambda_{\mathrm{c}} \propto 1/\sqrt{\alpha_{\mathrm{sp}}^{\mathrm{FC}}}$ and illustrate typical hysteresis loops as expected in materials with different types of pinning centers, where we normalize our results with $\lambda_{\mathrm{c}0} = (B_0^2/4\pi\alpha_0)^{1/2}$, α_0 the equilibrium Campbell curvature at $T = 0$.

D. Creep effect on the hysteresis loop in FC state

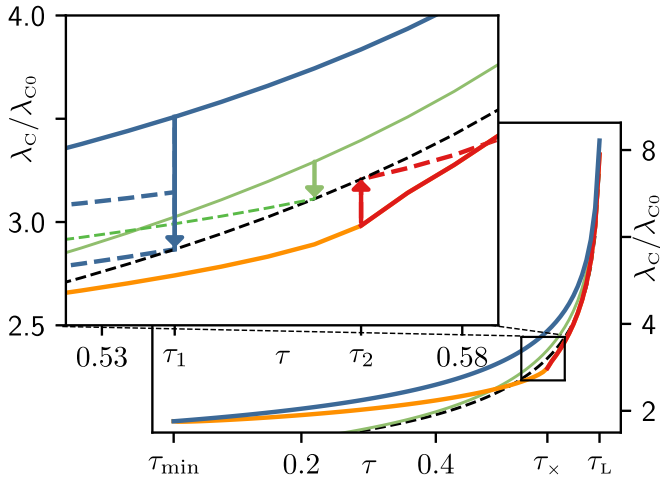We now proceed to include the effect of thermal fluctuations or creep on the Campbell length λ_{c} in the FC case.

FIG. 8. Hysteresis loop for the Campbell length λ_c measured along a temperature cycle $\tau_L \to \tau_{\min} \to \tau_L$. We assume insulating defects of Lorentzian form with a defect size $\rho/\xi_0 = 1.25$, that produces a maximum pinning parameter $\kappa(\tau_{\min}, b_0) \approx 8.3$, see Eq. (99), and $\tau_L \equiv T_L/T_c \approx 0.65$. We choose $\tau_{\min} = 0.01$ and a reduced magnetic field $b_0 = 0.05$. The Campbell length $\lambda_c(\tau)$ is normalized with respect to $\lambda_{c0} = (B_0^2/4\pi\alpha_0)^{1/2}$, α_0 the equilibrium Campbell curvature at $T = 0$. The cycle follows the phases b (blue) on cooling, a (orange) and b' (red) on heating, see also Fig. 6. For comparison, the Campbell length in the ZFC state (green solid line) is shown, as well as the equilibrium value (black dashed line). (Inset) Effect of creep on the Campbell length in the FC and ZFC states. The temperature range corresponds to the small black box in the main figure. At a temperature τ_1 during cooling, the FC state is relaxed (blue arrow) and approaches the equilibrium state, with the Campbell length gradually decreasing towards $\lambda_0(\tau)$. Resuming the cooling process at a later time, the Campbell length follows different trajectories (thick dashed blue) for different waiting times. Repeating this procedure at a temperature τ_2 along the warming branch, analogous results are found, with the Campbell length now increasing under the effect of creep (shown in red). Letting the system relax from the ZFC state (green arrow), the Campbell length approaches the equilibrium value λ_0 and behaves similar to the FC state upon further cooling (green dashed).

Thermal fluctuations drive the vortex state towards equilibrium, that corresponds to shifting the original position of the force jump towards x_0, thereby approaching the equilibrium distribution $p_{eq}(R) = \Theta(x_0 - R)$. This relaxation can be experimentally observed at any place along the temperature cycle, with a specific example (assuming insulating defects) shown in Fig. 8, by interrupting the temperature sweep and letting the system relax. Alternatively, creep tends to close the hysteresis loop when cycling the temperature at an ever slower rate. The relaxation of the FC states is largely different in the three phases a, b, and b' of the cycle: when the force jump is pinned to the edges x_- or x_+ in the phases b and b', the activation barriers are initially small (as they vanish at $x_\pm$) and hence relaxation is large. On the other hand, deep in the a phase, the jump location x_a^{jp} resides away from these edges and the initial barriers $U(x_a^{jp})$ are already large to start with, resulting in a slow relaxation. Nevertheless, there is an interesting crossover to the fast creeping b and b' phases at the edges of the a phase; in the following, we first focus

on relaxation of the phases b and b' and discuss the slow relaxation of phase a and its relation to the b and b' phases at the end.

Before deriving the expressions for the time evolved curvatures $\alpha^{FC}(t, T)$, we summarize our results in Fig. 8 on the example of a hysteretic cooling/warming hysteretic cycle as it appears for the insulating defect or for $\delta\ell$-pinning. Depending on which part of the temperature cycle the relaxation process takes place (by stopping the change in temperature), the Campbell length $\lambda_c(t, T)$ either grows or decreases in approaching the equilibrium state. The inset in Fig. 8 shows three cases, relaxation during the b phase (on cooling, in blue, with decreasing λ_c^b), at the end of the a phase/start of the b' phase (upon heating, in red, with increasing $\lambda_c^{b'}$), and relaxation of the ZFC state in green (decreasing λ_c). The various relaxation traces approach the equilibrium value $\lambda_c^0 \propto 1/\sqrt{\alpha_0}$ shown as a black dashed line. Stopping the relaxation by further cooling/heating, the penetration depth λ_c returns back to the FC lines (dashed blue/red lines). The relaxation in the a phase is slow away from its edges at $T_{\min}$ and $T_\times$ as the activation barriers become large. Hence, we find that combining cooling, heating, and relaxation allows us to install numerous different vortex states, permitting us to spectroscopize the pinning force and thus probe the pinning potential of defects in a material.

We now return back to the general discussion and derive the time evolution of the Campbell curvatures $\alpha^{FC}(t, T)$ for the phases b and b'. In describing the effect of creep on the Campbell curvature, we make heavy use of the results obtained in Sec. IV B; specifically, we can make use of the shifts $\delta x_\pm$ and $\delta r_{p\pm}$, $\delta r_{f\pm}$ of the vortex asymptotic and tip position as determined through the dimensionless thermal barrier $\mathcal{T}$ defined in Eq. (39).

Very close to the Labusch point $\kappa - 1 \ll 1$, the bistable region is symmetric around x_0 and the force jumps at x_- and x_+ are equal, hence, relaxation of the Campbell curvature along phases b and b' of the temperature cycle are the same to leading order and identical with the result Eq. (81) for the ZFC state with the properly chosen Labusch parameter $\kappa(T)$. The beyond leading-order correction (107) to the tip positions shifts the b and b' curves for the curvatures symmetrically down and up with respect to the ZFC result, see Fig. 9.

Going to lower temperatures, the pinning parameter κ grows larger and the equivalence between the FC curvatures α_{sp}^b and $\alpha_{sp}^{b'}$ and the ZFC result α_{sp} is lifted. Using the expression $\Delta f_{pin}^{fp}(x) = \bar{C}[r_f(x) - r_p(x)]$ to evaluate the force jumps, and dropping the pinned against the free vortex tip position, i.e., $r_f(x) \gg r_p(x)$ for $\kappa \gg 1$, we find that

$$\Delta f_{pin}^{jp,b} - \Delta f_{pin}^{fp}(x_-) \approx \bar{C}\,\delta r_{f-}, \tag{115}$$

$$\Delta f_{pin}^{jp,b'} - \Delta f_{pin}^{fp}(x_+) \approx -\bar{C}\delta r_{f+}, \tag{116}$$

where $\Delta f_{pin}^{jp,b} = \Delta f_{pin}^{fp}(x_-^{jp})$ and $\Delta f_{pin}^{jp,b'} = \Delta f_{pin}^{fp}(x_+^{jp})$. Combining these results for the force jumps with the renormalized trapping radii

$$x_b^{jp} = x_-(1 + \delta x_-/x_-), \tag{117}$$

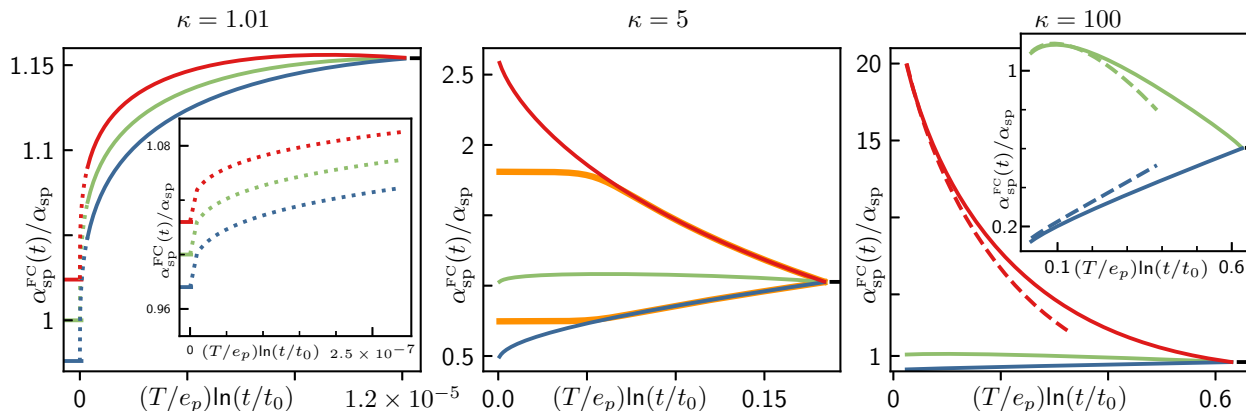$$x_{b'}^{jp} = x_+(1 - \delta x_+/x_+), \tag{118}$$

FIG. 9. Relaxation of the scaled Campbell curvature $\alpha_{sp}^{FC}(t)/\alpha_{sp}$ vs creep parameter $\mathcal{T} = (T/e_p) \ln(t/t_0)$. Shown are results for the field cooled (FC) phases b (in blue), b' (in red), and a (in orange, middle), as well as the zero-field cooled result (ZFC, green) for comparison. Assuming a Lorentzian pinning potential, we show results for marginally strong ($\kappa = 1.01$), intermediate ($\kappa = 5$), and very strong ($\kappa = 100$) pinning. Numerical results are shown as continuous lines, dashed lines (at large κ) describe analytic results at small values of $\mathcal{T}$. At marginally strong pinning ($\kappa = 1.01$, left), the relaxation curves for the phases b and b' separate symmetrically away from the ZFC result, a result obtained analytically only when going beyond leading order, see Eq. (107); the thick colored ticks marking the analytic results at $t = t_0$ agree well with the end points of the numerical curves (dotted lines show the extrapolation of the results to $t = 0$). The middle panel ($\kappa = 5$) also shows results for the a phase with a flat initial regime (slow relaxation) joining the trace [at time t_a, see Eq. (125)] for the b' (red) or b (blue) phase (depending on the starting point $x_0 < x_a^{jp} < x_+$ or $x_- < x_a^{jp} < x_0$, respectively) at large times. Analytic and numerical results agree well in the large κ limit and at small $\mathcal{T}$, with the results for the b (b') phases increasing (decreasing) monotonously with time, while the ZFC result is nonmonotonous. Note that the large values of $\alpha_{sp}^{b'}/\alpha_{sp}$ (red curve) require a large κ that is realized at low temperatures, typically. Thick ticks at large times mark the asymptotic value α_0/α_{sp} close to equilibrium $t \sim t_{eq}$ before entering the TAFF region, see text. The (numerical) lines terminate at the boundary of applicability $(T/e_p) \ln(t/t_0) \approx (\kappa - 1)^2/8$ and ~ 1 for marginally strong and very strong pinning, respectively. At very short times $t \sim t_0$, our creep analysis breaks down as the barriers U vanish.

the general expressions for the relaxation of the Campbell curvature during the phases b and b' of the temperature cycle assume the form [cf. Eq. (63) for the ZFC and note that $\delta r_{f+} \approx \delta x_+$; here, $\kappa = \kappa(T)$ is always chosen at the appropriate temperature T]

$$\frac{\alpha_{sp}^b(t, T)}{\alpha_{sp}^b} \approx \left(1 + \frac{\delta x_-}{x_-}\right)\left(1 + \frac{\delta r_{f-}}{r_{f-}}\right), \quad (119)$$

$$\frac{\alpha_{sp}^{b'}(t, T)}{\alpha_{sp}^{b'}} \approx \left(1 - \frac{\delta x_+}{x_+}\right)\left(1 - \frac{\delta r_{f+}}{x_+}\right). \quad (120)$$

We observe that, contrary to the situation in the ZFC state where we found a competition between an increasing trapping area and a decreasing force jump, in the FC states, the changes in the trapping area and in the force jumps work together. In particular, the trapping area *shrinks* with time in the b' phase. Hence, relaxing the state during phase b always leads to an increasing curvature, larger then the ZFC result, i.e., a decreasing Campbell penetration depth λ_c, while the opposite applies during phase b', see Fig. 9.

Focusing on the phase b for a Lorentzian potential, we can make use of the results (69) for δx_- and δr_{f-} and find that

$$\frac{\alpha_{sp}^b(t, T)}{\alpha_{sp}^b} \approx \left(1 + \frac{3}{8}\kappa^{1/3}(\sqrt{3}\mathcal{T})^{2/3}\right)$$

$$\times \left(1 + \frac{1}{2}\kappa^{1/6}(\sqrt{3}\mathcal{T})^{1/3}\right). \quad (121)$$

This result is valid at short times, where δr_{f-} is dominated by the square root behavior of the force profile close to x_-. Go-

ing beyond short times, such that $\delta x_- \gg x_-/6$, the deviation $\delta r_{f-} \approx r_{f-}/3 + \delta x_-$ is approximately linear, as discussed in the derivation of Eq. (64), and the Campbell curvature reads

$$\frac{\alpha_{sp}^b(t, T)}{\alpha_{sp}^b} \approx \left(1 + \frac{3}{8}\kappa^{1/3}(\sqrt{3}\mathcal{T})^{2/3}\right)$$

$$\times \left(1 + \frac{1}{3} + \frac{1}{2}\kappa^{1/3}(\sqrt{3}\mathcal{T})^{2/3}\right). \quad (122)$$

In the analysis of the relaxation during phase b', we proceed the same way: we make use of the result (69) for δx_+ and note that $\delta r_{f+} \approx \delta x_+$ to find the result

$$\frac{\alpha_{sp}^{b'}(t)}{\alpha_{sp}^{b'}} \approx \left(1 - \frac{\delta x_+}{x_+}\right)\left(1 - \frac{\delta x_+}{x_+}\right)$$

$$\approx (1 - 2(\sqrt{3}\mathcal{T})^{2/3} + (\sqrt{3}\mathcal{T})^{4/3}) \quad (123)$$

for the Lorentzian potential. With the above results, we find that the relaxation of the b and b' phases under FC conditions is always faster than the relaxation for a ZFC experiment, see Eqs. (72) and (73).

The upward (downward) relaxation of the Campbell curvatures $\alpha_{sp}^{b(b')}(t, T)$ is illustrated in Fig. 9, middle and right panels, with the curves $\alpha_{sp}^{b,b'}(t, T)$ (blue and red) enclosing the ZFC result $\alpha_{sp}(t, T)$ (green). This implies a reverse behavior in the Campbell penetration length λ_c, which decreases with time in the b phase and increases in the b' phase, see the example of a cooling-warming cycle for the case of insulating defects in Fig. 8.

Finally, we discuss the behavior of the a phase upon relaxation. The a phase can be entered either via the b phase [see, e.g., Fig. 6(b)], via the b' phase [see, e.g., Fig. 6(e)] very close to T_L, or directly from x_{0_L} at T_L [see Fig. 7(e)]. To fix ideas, here we focus on the situation where the a phase is entered from the b' phase; the jump location x_a^{jp} then resides in the interval $[x_0, x_+]$ and the (depinning) barrier $U_{\mathrm{dp}}(x_a^{\mathrm{jp}})$ is finite right from the start at t_0. Rather then reanalyzing this new situation 'microscopically', let us consider a substitute process where we start in the b' phase and let it decay in time (at the same point (τ, b_0) in phase space). Then, after a time t_a, the jump location $x_{b'}^{\mathrm{jp}}(t_a)$ will reach x_a^{jp} and from there on, the further decay of the b' phase traces the decay of the a phase. As a result, we find that

$$\alpha_{\mathrm{sp}}^a(t) = \alpha_{\mathrm{sp}}^{b'}(t + t_a) \tag{124}$$

with the waiting time t_a given by the usual estimate $T \ln(t_a/t_0) \approx U_{\mathrm{dp}}(x_a^{\mathrm{jp}})$ or

$$t_a \approx t_0 \exp\left[U_{\mathrm{dp}}(x_a^{\mathrm{jp}})/T\right]. \tag{125}$$

For the case where we enter the a phase from the b phase, we have to shift α_{sp}^b instead, $\alpha_{\mathrm{sp}}^a(t) = \alpha_{\mathrm{sp}}^b(t + t_a)$, and substitute $U_{\mathrm{dp}}(x_a^{\mathrm{jp}})$ by $U_{\mathrm{p}}(x_a^{\mathrm{jp}})$. In general, when $x_0 < x_a^{\mathrm{jp}} < x_+$, we shift $\alpha_{\mathrm{sp}}^{b'}$, while α_{sp}^b is to be shifted when $x_- < x_a^{\mathrm{jp}} < x_0$.

Translating the seemingly trivial linear-in-time shift $t \to t + t_a$ to the $\ln(t/t_0)$ plot of Fig. 9 produces an interesting outcome, see the orange line in the middle panel. With $x_a^{\mathrm{jp}} < x_+$, we have a smaller force jump Δf_{pin} and hence α_{sp}^a starts out at a lower value then the $\alpha_{\mathrm{sp}}^{b'}(t)$ curve, $\alpha_{\mathrm{sp}}^a(t_0) < \alpha_{\mathrm{sp}}^{b'}(t_0)$. Next, the slope $\partial_{\ln(t/t_0)}\alpha_{\mathrm{sp}}^a|_t$ at small times $t \ll t_a$ relates to the slope of $\alpha_{\mathrm{sp}}^{b'}$ at t_a, $\partial_{\ln(t/t_0)}\alpha_{\mathrm{sp}}^{b'}|_{t_a} \equiv -\alpha'$, via

$$\partial_{\ln(t/t_0)}\alpha_{\mathrm{sp}}^a\big|_t = t\,\partial_t\alpha_{\mathrm{sp}}^a\big|_t$$
$$= \frac{t}{t_a}\left[t\,\partial_t\alpha_{\mathrm{sp}}^{b'}\right]_{t_a} = -\frac{t}{t_a}\alpha' \tag{126}$$

and hence is small by the factor $t/t_a \ll 1$. As a result, we find that $\alpha_{\mathrm{sp}}^a(t)$ evolves flat in $\ln(t/t_0)$ and then bends over to $\alpha_{\mathrm{sp}}^{b'}(t)$ at $t \sim t_a$, see Fig. 9, within a ln-time interval of unit size or a $\mathcal{T}$-interval of order T/e_p, which is small on the extension $\mathcal{T} \approx 1$ of the creep parameter.

In an experiment, where the relaxation of the Campbell curvature (or length) is plotted versus ln-time, the a phase will start out with a seemingly slow decay (a flat curve) as compared to the decay of the b' phase, see Fig. 9. This is owed to the vanishing of the barrier for the b' phase at small times, hence the b' phase decays much faster than the a phase. Once the waiting time t_a is reached, the decay of the b' phase has slowed down such as to catch up with the decay of the a phase. The detection of the a phase in an experiment then depends on its time resolution: this will be successful if t_a resides within the observable time window of the relaxation experiment. If t_a is too large (note that $t_a \propto \exp[U(x_a^{\mathrm{jp}})/T]$ exponentially depends on the barrier and the temperature T) as compared to the time window of the measurement, only the flat part of the curve will be observed, with apparently no relaxation of the Campbell length. On the other hand, if t_a is too short to be caught by the experiment then one will

resolve a phase b' type relaxation and the feature appertaining to the a phase (flat part) is lost. The absence of relaxation in the Campbell length observed [18] in a BiSCCO sample finds a simple explanation in terms of large barriers that are present in the a phase of the hysteresis loop.

V. SUMMARY AND OUTLOOK

Strong pinning theory delivers a quantitative description of vortex pinning in the dilute defect limit. This fact is particularly prominent in the context of the Campbell ac response: not only can we describe a multitude of different vortex states, the zero-field cooled state and various types of field cooled states, we also can accurately trace the time evolution of these states and their signatures in Campbell penetration depth measurements. The strong pinning theory thus provides access to hysteretic and relaxation effects in the ac response that are otherwise, e.g., via weak collective pinning theory, at least so far, not available.

In this work, we have studied the effects of thermal fluctuations at finite temperatures T, or creep, on the Campbell penetration depth $\lambda_C \propto 1/\sqrt{\Delta f_{\mathrm{pin}}}$ that tracks the force jumps Δf_{pin} in the strong pinning landscape of Fig. 3. The proportionality $\alpha_{\mathrm{sp}} \propto \Delta f_{\mathrm{pin}}$, first found in Ref. [9], provides a satisfying connection to the curvature α appearing in Campbell's original [5] phenomenological description: the jump Δf_{pin} effectively averages the curvatures in the pinning landscape. Remarkably, ac penetration experiments provide new information on the pinning landscape, different from standard critical current density $j_c \propto \Delta e_{\mathrm{pin}}$ measurements that tell about the jumps Δe_{pin} in energy.

In our analysis of the zero-field cooled (ZFC) state, we found an interesting relaxation behavior of the Campbell curvature $\alpha_{\mathrm{sp}}(t, T)$ (or penetration depth $\lambda_C \propto 1/\sqrt{\alpha_{\mathrm{sp}}}$) with a nonmonotonous time-evolution at medium to large values of the pinning parameter κ, increasing first at small waiting times t and then decreasing towards a finite equilibrium value $\alpha_0 > 0$. At small values of $\kappa - 1 \ll 1$, the marginal strong pinning situation, we found the curvature $\alpha_{\mathrm{sp}}(t, T)$ rising monotonously; numerical analysis shows that nonmonotonicity appears at still rather small values of $\kappa \approx 2$. The decay to a finite value α_0 in the Campbell curvature is very different from the decay to zero of the persistent current density $j(t, T)$, a fact owed to the different limits of $\Delta f_{\mathrm{pin}} > 0$ and $\Delta e_{\mathrm{pin}} = 0$ at the branch crossing point x_0, see Fig. 3.

The relaxation of the field cooled (FC) states provides a rich variety of results as well: first of all, we find numerous types of hysteresis loops, depending on the characteristics of the defects, with insulating and metallic pointlike defects, δT_c and $\delta \ell$ pinning studied in more detail here, see also Ref. [12]. This different behavior is owed to the competition between an increasing $\kappa(T)$ and a decreasing $\xi(T)$ as the temperature T is decreased, with the scaling of $\kappa(T)$ determined by the type of pinning. Depending on the relative motion between the bistable interval $[x_-, x_+]$ (with $x_- \sim \kappa^{1/4}\xi$ and $x_+ \sim \kappa\xi$ at large κ) and the initial instability point $x_{0_L} = x_0(T_L)$ upon decreasing T, the jump location x^{jp} gets pinned at the edges $x_\pm(T)$ or stays put somewhere in between—these three cases define the phases b and b', as well as the a phase, that appear in the hysteresis loop when cycling the temperature down

and up. The appearance of these phases within a loop again depends on the defect type, with insulating defects and $\delta \ell$ pinning exhibiting all phases in the sequence b (cooling) to a (heating) to b' (heating), while the loops for δT_c pinning and metallic defects are dominated by the a phase. The three phases behave quite differently, with the b' phase providing a smaller penetration depth λ_c at large κ (where $\alpha_{sp}^b / \alpha_{sp}^{b'} \propto 1/\kappa^{3/2}$), while in terms of creep, the a phase sticks out by its slower decay. Further experimental signatures for these phases are the decay (increase) in magnitude of λ_c under creep for the b (b') phases and a plateau, i.e., an initially much slower relaxation (both up or down is possible) in the a phase due to the presence of large thermal barriers. Such characteristic differences then allow to make conjectures about the underlying pinning landscape.

In the present work, we have made an additional step towards better precision in our analytic results. Using the Lorentzian-shaped potential describing a pointlike defect as an example, we have provided analytic results including numerical factors; this further illustrates the value of the strong pinning concept as a quantitative theory. Furthermore, care has been taken to properly treat the trapping geometry of strong pinning, see Fig. 1. It turns out that this geometry affects transport and ac response in different ways: while in transport only the transverse trapping length $t_\perp = 2x_-$ shows up, when dealing with the (ZFC) ac response, pinning (involving a semi-circle of radius x_-) and depinning (at a circular segment of radius x_+) are weighted with separate factors. Furthermore, in the FC situation, trapping always appears on a circle with a radius $R \in [x_-, x_+]$ spanning the entire bistable region, depending on the induced vortex state; this feature has been missed in our previous analysis [12].

Several of the predictions made in the present work have been observed in experiments measuring the Campbell pene-tration length. Examples are the decreasing $\lambda_c(t)$ in a BiSCCO sample [18] that is consistent with an increasing Campbell curvature at short times or marginally strong pinning, see Fig. 4, the increasing $\lambda_c(t)$ in an YBCO superconductor [19] that is consistent with the long time behavior of the Campbell curvature at intermediate and very strong pinning, see again Fig. 4, the finite equilibrium value of the Campbell length λ_{c0}, see Eq. (84), that has been observed in a BiSCCO sample above the irreversibility line, and the absence of creep in the field cooled (FC) state of a BiSCCO single crystal [18], here explained in terms of an a phase that is characterized by the presence of large barriers, see also Fig. 9.

In the present study, we have focused on the low-field regime where the trapping length x_+ stays below the vortex lattice constant, $x_+ < a_0/2$. At larger field values, multiple vortices start competing for the same defect and our single-pin–single-vortex description has to be extended to include several vortices, see also Refs. [22,23]. This becomes particularly relevant in very anisotropic and layered material with $\varepsilon \ll 1$, where $\kappa \propto 1/\varepsilon$ can become large and $x_+ \sim \kappa \xi$ easily goes beyond $a_0/2$ even at moderate field values already. Related to the possibility of such very strong pinning is the prediction [30] of a creep-*enhanced* critical current due to a dominant increase in the trapping area at very large κ. Furthermore, since pinning remains active also beyond [20] j_c it would be interesting to measure and analyze the Campbell penetration physics in the dynamical vortex state.

[1] A. Abrikosov, On the magnetic properties of superconductors of the second group, Sov. Phys. JETP **5**, 1174 (1957).

[2] A. Campbell and J. Evetts, Flux vortices and transport currents in type ii superconductors, Adv. Phys. **21**, 199 (1972).

[3] M. Tinkham, *Introduction to Superconductivity*, Dover Books on Physics Series (Dover Publications, 2004).

[4] P. G. De Gennes, *Superconductivity of Metals and Alloys*, Advanced Book Classics (Perseus, Cambridge, MA, 1999).

[5] A. M. Campbell, The response of pinned flux vortices to low-frequency fields, J. Phys. C **2**, 1492 (1969).

[6] R. Labusch, Calculation of the critical field gradient in type-ii superconductors, Cryst. Lattice Defects **1**, 1 (1969).

[7] A. I. Larkin and Y. N. Ovchinnikov, Pinning in type-II superconductors, J. Low Temp. Phys. **34**, 409 (1979).

[8] G. Blatter, V. B. Geshkenbein, and J. A. G. Koopmann, Weak to Strong Pinning Crossover, Phys. Rev. Lett. **92**, 067009 (2004).

[9] R. Willa, V. B. Geshkenbein, R. Prozorov, and G. Blatter, Campbell Response in Type-II Superconductors Under Strong Pinning Conditions, Phys. Rev. Lett. **115**, 207001 (2015).

[10] J. Lowell, Investigation of pinning centres in superconductors by means of alternating currents. i. theory, J. Phys. F **2**, 547 (1972).

[11] A. Campbell, The pinning of flux lines in superconductors by randomly-spaced pinning centres, Philos. Mag. B **37**, 149 (1978).

[12] R. Willa, V. B. Geshkenbein, and G. Blatter, Probing the pinning landscape in type-II superconductors via campbell penetration depth, Phys. Rev. B **93**, 064515 (2016).

[13] C. P. Bean, Magnetization of Hard Superconductors, Phys. Rev. Lett. **8**, 250 (1962).

[14] M. Buchacek, R. Willa, V. B. Geshkenbein, and G. Blatter, Persistence of pinning and creep beyond critical drive within the strong pinning paradigm, Phys. Rev. B **98**, 094510 (2018).

[15] M. Buchacek, R. Willa, V. B. Geshkenbein, and G. Blatter, Strong pinning theory of thermal vortex creep in type-II superconductors, Phys. Rev. B **100**, 014501 (2019).

[16] A. U. Thomann, V. B. Geshkenbein, and G. Blatter, Dynamical Aspects of Strong Pinning of Magnetic Vortices in Type-II Superconductors, Phys. Rev. Lett. **108**, 217001 (2012).

[17] M. Buchacek, Z. L. Xiao, S. Dutta, E. Y. Andrei, P. Raychaudhuri, V. B. Geshkenbein, and G. Blatter, Experimental test of strong pinning and creep in current-voltage characteristics of type-ii superconductors, Phys. Rev. B **100**, 224502 (2019).

[18] R. Prozorov, R. W. Giannetta, N. Kameda, T. Tamegai, J. Schlueter, and P. Fournier, Campbell penetration depth of a superconductor in the critical state, Phys. Rev. B **67**, 184501 (2003).

[19] G. Pasquini and V. Bekeris, Thermal annealing of the torn vortex lattice in YBa$_2$Cu$_3$O$_7$ crystals, Phys. Rev. B **71**, 014510 (2005).

[20] A. U. Thomann, V. B. Geshkenbein, and G. Blatter, Vortex dynamics in type-II superconductors under strong pinning conditions, Phys. Rev. B **96**, 144516 (2017).

[21] W.-K. Kwok, U. Welp, A. Glatz, A. E. Koshelev, K. J. Kihlstrom, and G. W. Crabtree, Vortices in high-performance high-temperature superconductors, Rep. Prog. Phys. **79**, 116501 (2016).

[22] R. Willa, A. Koshelev, I. Sadovskyy, and A. Glatz, Strong-pinning regimes by spherical inclusions in anisotropic type-ii superconductors, Supercond. Sci. Technol. **31**, 014001 (2018).

[23] R. Willa, A. E. Koshelev, I. A. Sadovskyy, and A. Glatz, Peak effect due to competing vortex ground states in superconductors with large inclusions, Phys. Rev. B **98**, 054517 (2018).

[24] G. Blatter, M. V. Feigel'man, V. B. Geshkenbein, A. I. Larkin, and V. M. Vinokur, Vortices in high-temperature superconductors, Rev. Mod. Phys. **66**, 1125 (1994).

[25] J. Bardeen and M. J. Stephen, Theory of the motion of vortices in superconductors, Phys. Rev. **140**, A1197 (1965).

[26] S. Brazovskii and A. Larkin, Nonlinear conduction of sliding electronic crystals: Charge and Spin Density Waves, J. Phys. IV (France) **09**, Pr10 (1999).

[27] S. Brazovskii and T. Nattermann, Pinning and sliding of driven elastic systems: from domain walls to charge density waves, Adv. Phys. **53**, 177 (2004).

[28] P. H. Kes, J. Aarts, J. van den Berg, C. J. van der Beek, and J. A. Mydosh, Thermally assisted flux flow at small driving forces, Supercond. Sci. Technol. **1**, 242 (1989).

[29] R. Willa, V. B. Geshkenbein, and G. Blatter, Campbell penetration in the critical state of type-II superconductors, Phys. Rev. B **92**, 134501 (2015).

[30] F. Gaggioli, G. Blatter, and V. Geshkenbein, Enhancing the pinning force density by thermal creep (unpublished).

[31] M. W. Coffey and J. R. Clem, Theory of rf magnetic permeability of isotropic type-ii superconductors in a parallel field, Phys. Rev. B **45**, 9872 (1992).

[32] C. J. van der Beek, V. B. Geshkenbein, and V. M. Vinokur, Linear and nonlinear ac response in the superconducting mixed state, Phys. Rev. B **48**, 3393 (1993).